Quaternary Science Reviews 224 (2019) 105946

Contents lists available at ScienceDirect

Quaternary Science Reviews

journal homepage: www.elsevier.com/locate/quascirev

Orbital-to-millennial scale climate variability during Marine Isotope Stages 5 to 3 in northeast Iberia

Carlos Pérez-Mejías [a, b, c, *], Ana Moreno [b], Carlos Sancho [c, 1], Rebeca Martín-García [d], Christoph Spötl [e], Isabel Cacho [f], Hai Cheng [a, g], R. Lawrence Edwards [g]

[a] Institute of Global Environmental Change, Xi'an Jiaotong University, Xi'an, 710049, China
[b] Department of Geoenvironmental Processes and Global Change, Pyrenean Institute of Ecology — CSIC, Avda. Montañana 1005, 50059, Zaragoza, Spain
[c] Earth Sciences Department, University of Zaragoza, C/Pedro Cerbuna 12, 50009, Zaragoza, Spain
[d] Station d'Ecologie Théorique et Expérimentale UMR 5321, CNRS, 2 route du CNRS, 09200, Moulis, France
[e] Institute of Geology, University of Innsbruck, Innrain 52, 6020, Innsbruck, Austria
[f] Dept. Dinàmica de la Terra i de l'Oceà, Facultat de Ciències de la Terra, Universitat de Barcelona, C/Martí Franques s/n, 08028, Barcelona, Spain
[g] Department of Earth and Environmental Sciences, University of Minnesota, John T. Tate Hall, 116 Church Street SE, Minneapolis, MN, 55455, USA

A R T I C L E I N F O

Article history:
Received 8 May 2019
Received in revised form
14 September 2019
Accepted 14 September 2019
Available online 4 October 2019

Keywords:
Stalagmite
Stable isotopes
Orbital-millennial scale
Last glacial period
Western mediterranean

A B S T R A C T

The climate during the last glacial cycle was characterized by abrupt millennial-scale changes superimposed on long-term orbital control. This study examines this climate variability for northeast Iberia for the time interval 118.9 to 36.9 kyr using a multi-proxy approach ($\delta^{18}O$, $\delta^{13}C$ and Mg/Ca) applied to a stalagmite that covers this period continuously. During Marine Isotope Stage (MIS) 5 and 4, $\delta^{18}O$ is controlled by orbital pacing, whereby more humid conditions prevailed during minima in boreal summer precession. In contrast, during MIS 3 $\delta^{18}O$ lags precession and co-varies with $\delta^{13}C$ ($\rho = 0.53$, p-value < 0.001, $n = 500$), suggesting a common control of both isotopes by reduced precipitation during dry periods. $\delta^{13}C$ shows a positive correlation with Mg/Ca, reflecting water availability, vegetation productivity and microbial activity in the catchment of the cave's drip water. The $\delta^{13}C$ values exhibit a response to Heinrich Stadials (HS) and other cold marine events (e.g. C26 to C23), as well as Dansgaard-Oeschger oscillations (D-O). The Last Interglacial ended at 108.6 ± 0.3 kyr at this site. Two periods with a marked "W-shape" pattern in $\delta^{13}C$ can be recognized between 70 and 50 kyr (hereafter multi-event). The older multi-event (including HS-6 and D-O 18) is characterized in the North Atlantic by high IRD discharges and cold sea-surface temperatures, while the two phases attending to the hydrology in the study area suggest dry conditions prior to HS-6. A dry climate prevailed during the younger multi-event (including HS-5a and D-O 15), coincident with an increase in productivity-related foraminifera species at lower latitudes, suggesting a reinforcement of the trade winds associated with a stronger Hadley Cell.

1. Introduction

Rapid abrupt changes characterized the climate during the Last Glacial period. The Dansgaard-Oeschger (D-O) cycles were the most notable expression of the atmospheric changes over Greenland, while massive iceberg discharges (Heinrich Stadials) represented a notable feature in the North Atlantic (Hemming, 2004). D-O oscillations involve swings between cold (stadial) and warm (interstadial) conditions on decadal timescales. Their origin is controversial (Lynch-Stieglitz, 2017) and the main paradigm relates those oscillations to changes in the northward transport of heat by the Atlantic Meridional Overturning Circulation (AMOC) (Rahmstorf, 2002). Potential disruptions in the AMOC have been identified during Heinrich events, identified by layers of ice-rafted debris that represent surges of the ice sheet that covered North America (Ruddiman, 1977; Rahmstorf, 2002; Hemming, 2004; Lynch-Stieglitz et al., 2014). Recently, the efforts have been focused on identifying the coupled atmosphere-ice-ocean dynamics within the Northern Seas, where three key elements interact: vigorous winds, sea ice and an oceanic gyre that connects the surface and deep ocean (Li and Born, 2019).

* Corresponding author. Institute of Global Environmental Change, Xi'an Jiaotong University, Xi'an, 710049, China.
E-mail address: perezmegias@mail.xjtu.edu.cn (C. Pérez-Mejías).
[1] deceased.

https://doi.org/10.1016/j.quascirev.2019.105946
0277-3791/

The impact of D-O events was not global, and speleothems from mid-latitudes such as North America (Springer et al., 2014; Lachniet et al., 2014) and Japan (Mori et al., 2018) and low-latitudes such as the Bahamas or Borneo (Arienzo et al., 2015; Carolin et al., 2016) do not record any response to these events.

Previous studies on the Iberian Margin (IM) (Sánchez-Goñi et al., 2008; Naughton et al., 2009; Margari et al., 2010) and in the Mediterranean Sea, including the Alborán Sea (Sánchez-Goñi et al., 2002; Moreno et al., 2002; Sierro et al., 2005; Fletcher and Sánchez-Goñi, 2008) and the Balearic Sea (Frigola et al., 2008), emphasize the potential of the paleorecords from the Iberian Peninsula (IP) to evaluate the response to climate change in the North Atlantic realm. In this regard, it is worth noting the pioneer studies in the Western Mediterranean that identified Heinrich events and cold stadials (Moreno et al., 2002) and the interruption of the antiphase relationship in deep-water formation between the North Atlantic and the Mediterranean (Sierro et al., 2005), as well as the vegetation response to the alternation between dry-cold conditions during D-O stadials, and to humid-mild conditions during the interstadials (Sánchez-Goñi et al., 2002). Unfortunately, only few published marine records extend beyond 50 kyr, thus limiting our understanding about the onset of the last glaciation and D-O variability (Frigola et al., 2008; Margari et al., 2009; Fletcher et al., 2010) and none of them provides an independent absolute chronology, with the exception of the last interglacial record of Tzedakis et al. (2018).

Our knowledge of the terrestrial response in Europe to millennial-scale changes from MIS 5 to MIS 3 has significantly increased during the last decade, but is still based on few key records. Lacustrine sediments from Europe covering this time period are scarce (Sirocko et al., 2005; Veres et al., 2009) with the exception of the long lacustrine sequences of Lago Grande di Monticchio, Fuccino, Ohrid and Tenaghi Philippon, anchored by tephra datings (Vogel et al., 2010; Martin-Puertas et al., 2014; Wulf et al., 2018; Mannella et al., 2019). Speleothems cover only short or discontinuous periods of time (Wainer et al., 2011, 2013; Fankhauser et al., 2016; Atsawawaranunt et al., 2018; Lechleitner et al., 2018; Weber et al., 2018; Budsky et al., 2019). Therefore, there is clearly a need for long, well-dated terrestrial records to explore the mechanisms of climate change at different timescales during the Last Interglacial (LIG) and the Last Glacial period. Here, we present a stalagmite record from Ejulve cave, northeastern Iberia, covering the period between the end of the LIG and MIS 3. In contrast to many other speleothems from European caves which preferentially formed during warm/wet periods and commonly stopped growing when the climate turned cold/dry (e.g., Genty et al., 2010; Boch et al., 2011; Vansteenberge et al., 2016; Wainer et al., 2011, 2013), this record is continuous and hence provides exceptional insights into the terrestrial mid-latitude response to forcing mechanisms across several climate transitions.

2. Study area

Ejulve cave (40°45′34′N, 0°35′07″W, 1240 m a.s.l.) is located in the Iberian Range, NE Spain (Fig. 1). The cave developed in folded and thrusted Upper Cretaceous dolomitic limestones and dolostones and comprises 794 m of galleries, reaching a maximum depth of 55 m. The thickness of the rock above the cave in the shallow areas is less than 10 m. Further details of the cave site can be found in Pérez-Mejías et al. (2019). The area above the cave is covered by poorly developed soil composed by patchy aridisols with shallow and stony soils supporting a vegetation composed mainly of sparse evergreen oak (*Quercus coccifera, Quercus ilex*), heliophytic shrubs (*Genista scorpius, Thymus vulgaris,* and sparse *Sideritis spinulosa* and *Rosmarinus officinalis*) and *Pinus halepensis*.

The local climate is continental Mediterranean, with a mean annual rainfall of 547 mm (1981–2010). The mean annual temperature is 12 °C ($\sigma = 6$) (2003–2012), with a mean temperature of 7 °C ($\sigma = 3$) in winter and 20 °C ($\sigma = 2$) in summer, with high evapotranspiration from March to October (Pérez-Mejías et al., 2018). The synoptic patterns of the present-day precipitation in the study area can be classified into three types: Atlantic fronts, back-door cold fronts and convective precipitation storms (Moreno et al., 2014). While the Atlantic fronts carry precipitation mostly to the western side of the Iberian Range, the back-door fronts involve complex mesoscale convective systems, involving Mediterranean cyclogenesis that provoke intense rainfall on the eastern side of the mountain range. Finally, convective precipitation is related to the formation of the Iberian thermal low, triggering orographic or convective storms (Moreno et al., 2014). The cave location is also influenced by atmospheric circulation patterns such as the North Atlantic Oscillation (NAO) and the Western Mediterranean Oscillation (WeMO). The preliminary study of Moreno et al. (2014) using a rainfall dataset of 3 years, suggests a statistically significant positive correlation between the amount of winter precipitation and the NAO index (linked to rainfall by Atlantic fronts), and a moderate one between $\delta^{18}O$ of precipitation and the WeMO in spring and summer (mostly linked to back-door fronts).

3. Methods

The studied stalagmite (dubbed ANDROMEDA), 41 cm long, was collected in-situ in Ejulve cave (Fig. 2A, B) and was cut along the growth axis with a diamond saw and polished. A total of 739 samples were micro-milled along the extension axis for stable isotope analysis, 558 samples of them in a continuous sampling mode at 0.2 mm increments (from 220 to 335 mm), and the remaining 181 samples (from 40 to 219 mm) at 1 mm resolution. For trace metals, 296 samples were sampled at 1 mm increments (from 40 to 335 mm). 26 samples were drilled for U-Th at different intervals focusing on potential hiatuses and slow-growth periods. Thin sections covering the whole stalagmite were examined using transmitted-light microscopy. X-ray diffraction (XRD) analyses were performed on five samples at the Jaume Almera Institute (ICTJA-CSIC) using a Bruker-AXS D5005 powder diffractometer configured in theta-2 theta geometry. Samples were also examined on palladium-coated slabs using a field emission scanning electron microscope (FE-SEM, CSEM-FEG INSPECT 50) equipped with an EDX detector at the Advanced Microscopy Laboratory-INA (Zaragoza). Epifluorescence observations of the thin sections were performed at the Theoretical and Experimental Ecology Station (CNRS) using a fluorescence stereo microscope (ZEISS Axio Zoom V16) with a HXP 200C illuminator.

Stable isotope analyses of the high-resolution interval (0.2 mm increments) were performed at the University of Innsbruck using a ThermoFisher Delta V Plus mass spectrometer linked to a Gasbench II, following the methodology described in Spötl (2011). The remaining samples were analyzed at the University of Barcelona using a Finnigan MAT 252 mass spectrometer, equipped with a Kiel Carbonate Device III, reproducing a modified version of the McCrea method (McCrea, 1950). Carbonate is attacked with 100% phosphoric acid at 70 °C, with a 5 min reaction time. Values are reported as $\delta^{18}O$ (‰) and $\delta^{13}C$ (‰) with respect to the Vienna Pee Dee Belemnite (V-PDB) standard. Long-term precision for $\delta^{13}C$ and $\delta^{18}O$ (1σ) was 0.06‰ and 0.08‰ for the Innsbruck laboratory and 0.04‰ and 0.08‰ for the Barcelona laboratory, respectively. Calibration of the raw results versus the V-PDB scale was achieved using in-house calcite standards calibrated against NBS-18, NBS-19, CO-1 and CO-8 reference materials. Trace-metal analysis was performed in the IPE-CSIC laboratories using an ICP-AES (ThermoFisher iCAP DUO 6300)

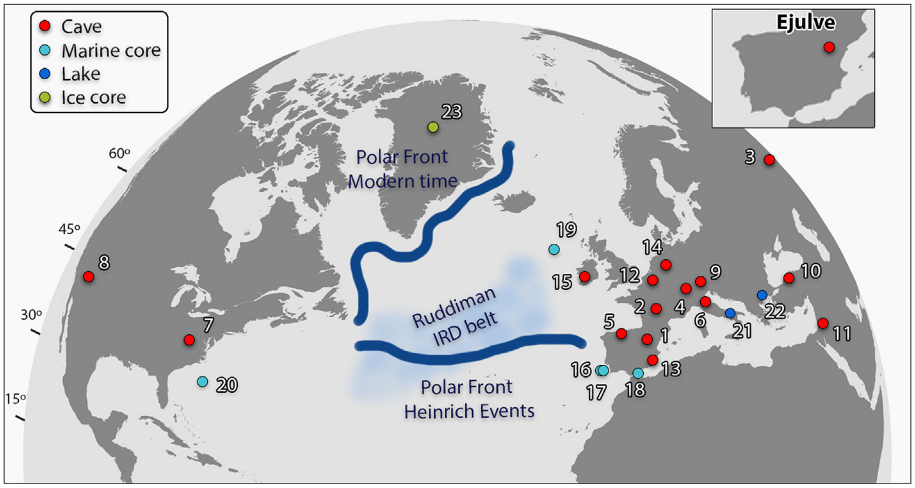

Fig. 1. Location of Ejulve cave and records discussed in the text, corresponding to: 1. Ejulve (present study), 2. Villars (Genty et al., 2010, 2003), 3. Chinese composite (Cheng et al., 2016), 4. NALPS (Boch et al., 2011; Moseley et al., 2014), 5. Asturian caves (Stoll et al., 2013), 6. Corchia (Drysdale et al., 2007; Tzedakis et al., 2018), 7. BCC (Springer et al., 2014), 8. Leviathan (Lachniet et al., 2014), 9. Entrische Kirche (Meyer et al., 2008), 10. Sofular (Fleitmann et al., 2009), 11. Soreq (Bar-Matthews et al., 2003), 12. Han-sur-lesse (Vansteenberge et al., 2016), 13. Cueva Victoria (Budsky et al., 2019), 14. Bunker (Weber et al., 2018), 15. Crag (Fankhauser et al., 2016) (caves), 16. MD95-2042 (Sánchez-Goñi et al., 2017), 17. MD01-2444 (Vautravers and Shackleton, 2006; Martrat et al., 2007), 18. ODP-976 (Martrat et al., 2014), 19. IODP U1308 (Hodell et al., 2008), 20. ODP 172–1060 (Vautravers et al., 2004) (marine cores), 21. Monticchio (Allen and Huntley, 2009; Martin-Puertas et al. (2014), 22. Tenaghi Phillippon (Wulf et al., 2018) (lakes) and 23. NGRIP (North Greenland Ice Core Project members, 2004) (ice core). The position of the polar front is marked for the present day (Dickson et al., 1988) and reconstructed for Heinrich events (Eynaud et al., 2009; Voelker and Abreu, 2011).

using molar Mg/Ca ratios. Approximately 1 mg of sample was dissolved in 2% HNO_3, following the procedure described in Moreno et al. (2010). U-Th samples were analyzed using a MC-ICP-MS (ThermoFisher Neptune Plus) at the University of Minnesota and at the Xi'an Jiaotong University following the methodology described in Cheng et al. (2013). The ages are expressed in years before present (BP). The depth-age model was constructed using OxCal, with a P_sequence deposition model (Ramsey, 2008).

4. Results

4.1. Petrography and mineralogy

ANDROMEDA is 41 cm long, 9 cm wide at the base and 5 cm wide at the top, showing a conical external shape (Fig. 2A). It is composed of radiating columnar calcite crystals showing macroscopically visible laminae in the lower half of the stalagmite, although the laminae have limited lateral continuity.

ANDROMEDA is composed of calcite and no other minerals were identified by XRD. Thin sections reveal a fabric of polycrystals 11–20 mm long and 3–5 mm wide (L/W ratio below 6:1) showing uniform extinction with patches (Fig. 2C). The smaller crystals forming the polycrystals are 1–7 mm long and about 1 mm wide. The intercrystalline borders are irregular and the fabric is compact and shows low porosity (Fig. 2D). These characteristics correspond to the columnar microcrystalline fabric described by Frisia (2015).

All thin sections show weak homogeneous epifluorescence with no evidence of layering or changes in composition (Fig. 2E). In the upper part, hiatus 3 (Fig. 3) is marked by a micritic layer showing more intensive fluorescence. FE-SEM images of freshly broken surfaces reveal a homogeneous calcite fabric. EDX point analyses of the polished surfaces indicate low-Mg calcite.

4.2. Age model and growth rate

The chronology of ANDROMEDA is anchored by 26 U-Th ages (Table 1), with analytical errors between 2 and 4‰. ^{232}Th is general lower than 500 ppt. The ^{238}U content is mostly between 100 and 200 ppb, similar to values of other stalagmites in this cave (Moreno et al., 2017; Pérez-Mejías et al., 2017). The depth-age model was constructed using 21 U-Th ages between hiatus 1 and 2 (Fig. 3). The mean uncertainty of the record is of 162 yr (minimum 14 yr, maximum 641 yr). Five samples (in italics in Table 1) were not used since they are outside the studied interval.

The stalagmite exhibits three hiatuses, two of them (no. 2 and 3, Fig. 3) are visible with the naked eye and are confirmed by U-Th ages. Hiatus no. 1 is located close to the base of the stalagmite and shows no clear visible expression. Hiatus 2 spans from 36.9 ± 0.11 to 13.9 ± 0.04 kyr, and hiatus 3 from 10.8 ± 0.15 to 5.1 ± 0.03 kyr. In the present work we discuss data from 40 mm (post hiatus 1) until 340 mm above the base (before hiatus 2), from 119 to 36 kyr.

Growth rate ranges from 1 mm/kyr during 96–81 kyr to 11.6 mm/kyr during 81–76 kyr with a mean of 5.2 mm/kyr (Fig. 3). Overall, four stages of slow growth are separated by three phases of fast growth (Fig. 3). The former span 119-113 kyr, 99-81 kyr, 76-52 kyr and 46-36 kyr, corresponding to MIS 5e-d, 5b, 4 and the cold spells of MIS 3 (e.g. Greenland Stadials 9, 10, 11 of Rasmussen et al., 2014). The fast growth periods span 113-99 kyr, 81-76 kyr and 52-45 kyr (slightly lower during 48–46 kyr), corresponding to MIS 5c, 5a and 3 (Fig. 3).

4.3. Isotope and trace-metal geochemistry

The resolution of the stable isotope data varies between 22 years during the fast growth period of MIS 3 (52-45 kyr) and 1000 years during the slow growth phase of MIS 5b (99-81 kyr, Fig. 3). The average resolution is 109 years.

The $\delta^{18}O$ record of ANDROMEDA, corrected for the ice-volume effect (cf. Bintanja et al., 2005, Fig. 4), shows values between −9.17 and −6.51‰ (mean -8.08 ± 0.38‰). $\delta^{13}C$ values range from −9.97 to −3.25‰ (mean -7.24 ± 1.48‰). The highest and lowest $\delta^{18}O$ values occur during MIS 5 (117 and 107 kyr, respectively) (Fig. 5a). The lowest $\delta^{13}C$ values were also reached during this time interval (118 kyr), while the highest values occurred at 39 kyr (Fig. 5b).

The isotopic variability shows marked changes during the long

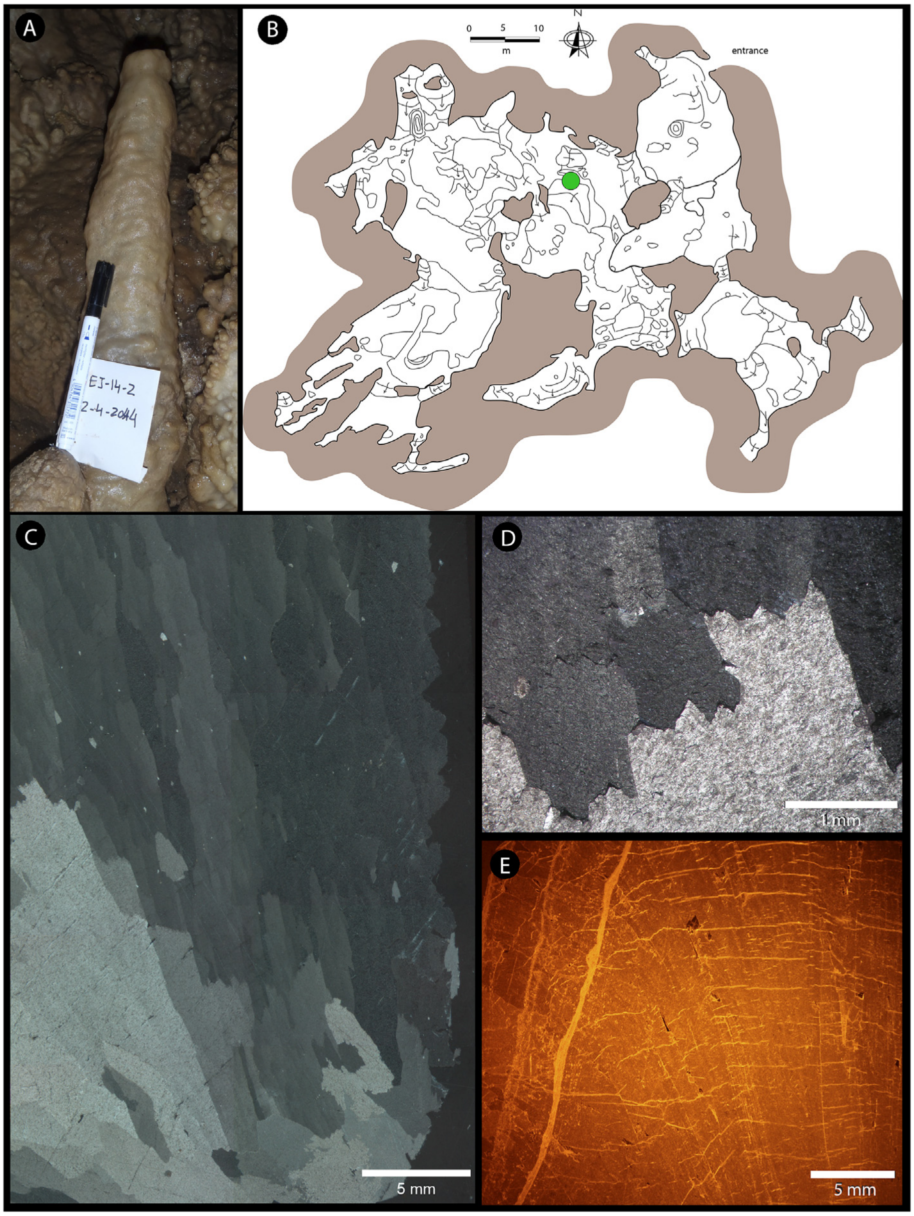

Fig. 2. A. ANDROMEDA stalagmite in growth position in the cave. B. Plan view of Ejulve cave and location of the sampled stalagmite (green symbol). C. Photomicrograph showing columnar calcite with uniform extinction (crossed nicols). D. Serrated intercrystalline boundaries (crossed nicols). E. Epifluorescence image of the calcite crystals. (For interpretation of the references to color in this figure legend, the reader is referred to the Web version of this article.)

growth history of the stalagmite. During MIS 4 and 3, the variability in $\delta^{18}O$ is 1.59‰ compared to 2.66‰ during MIS 5. In contrast, $\delta^{13}C$ shows the highest variability during the D-O oscillations of MIS 4 and 3 (5.62‰), while the variability during MIS 5 was lower (3.30‰). $\delta^{18}O$ and $\delta^{13}C$ show a variable degree of covariation along the growth axis, with no correlation during MIS 5 ($\rho = 0.01$, p-value = 0.83, n = 235) and a statistically significant correlation ($\rho = 0.53$, p-value < 0.001, n = 500) in MIS 4 and 3, indicating a different pattern between both periods.

The Mg/Ca ratio (Fig. 5c) shows a highly positive correlation with $\delta^{13}C$ ($\rho = 0.75$, p-value = 0.02, n = 295), notably in the MIS 4 and 3 sections (Fig. 5). In spite of the low resolution of the $\delta^{234}U$ record, high values co-vary with high values in Mg/Ca (Fig. 5d).

5. Discussion

5.1. Mineralogy and petrography

XRD analyses indicate that ANDROMEDA is entirely composed of calcite. Its columnar fabric is widely considered as a primary fabric of speleothems (Frisia et al., 2018), most likely associated with near-equilibrium conditions (Frisia et al., 2000). Some studies, however, have shown that this fabric could also be a result of early diagenesis, potentially resetting the original geochemical signals (Martín-García et al., 2009; Frisia and Borsato, 2010; Fairchild and Baker, 2012; Scholz et al., 2014; Bajo et al., 2016; Domínguez-Villar et al., 2017). In order to rule out this possibility, we used epifluorescence microscopy and SEM. Thin sections examined using epifluorescence, covering the whole length of the speleothem, showed a homogeneous orange color, typical of calcite. In contrast,

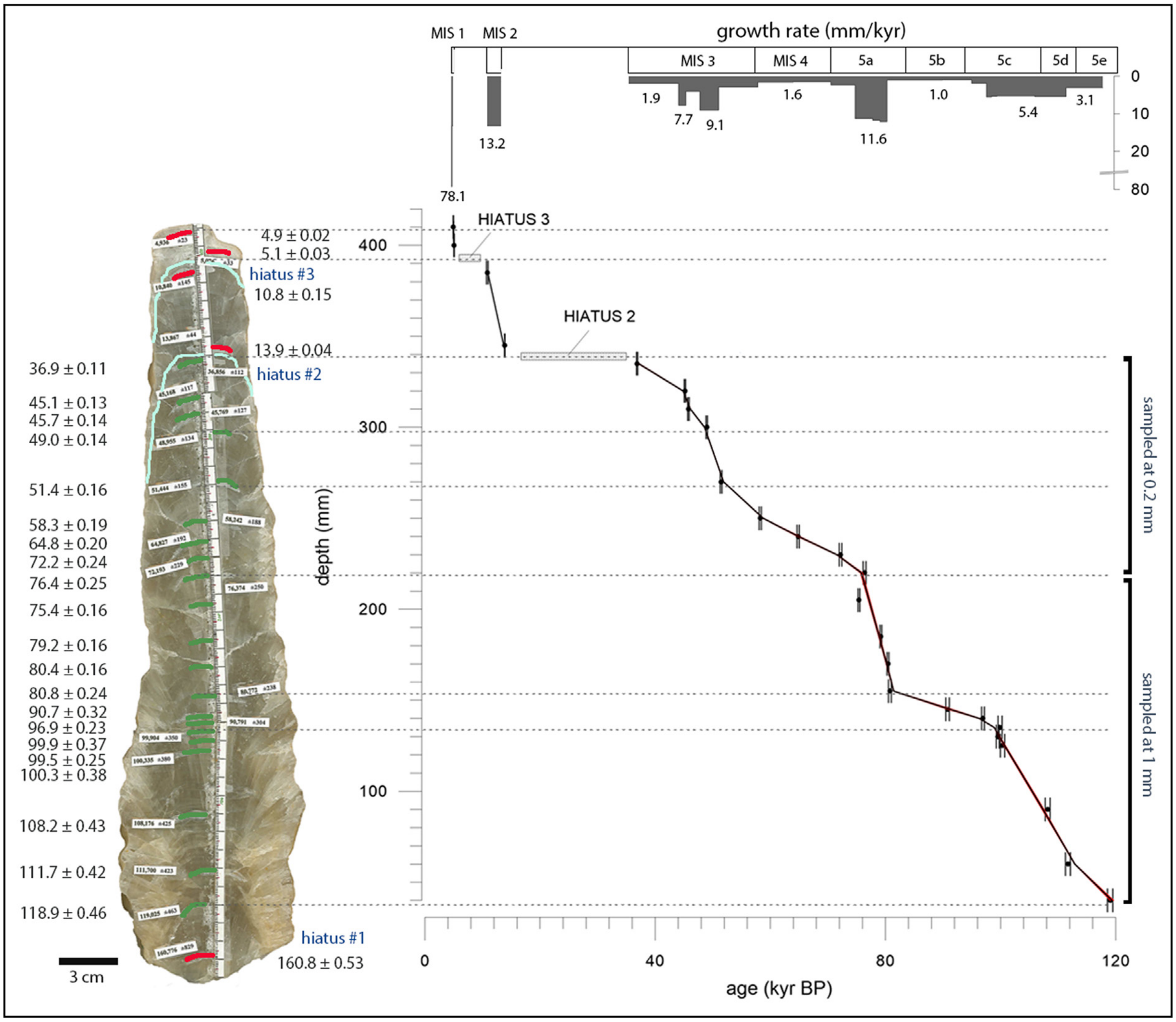

Fig. 3. Age model of ANDROMEDA for the interval between hiatuses 1 and 2. Samples marked in green were used to construct the depth-age model. Samples in red were dismissed. Hiatuses are highlighted by blue lines, except for hiatus 1 which is not visible macroscopically. Also shown are changes in growth rate. Age model and uncertainty are shown in red. The error bars are 2σ. Please note the two different intervals of sampling for isotope analysis. (For interpretation of the references to color in this figure legend, the reader is referred to the Web version of this article.)

aragonite typically shows blue fluorescence (Ortega et al., 2005; Pickering et al., 2010). SEM images of freshly broken surfaces showed no aragonite-related textures (i.e. no acicular, elongated columnar or whiskers (Frisia and Borsato, 2010)). In addition, the well-preserved lamination as well as the correct stratigraphic order of the U-Th dates also suggest that the columnar fabric is of primary origin. In essence, we find no evidence of diagenesis and therefore consider the proxy data as reliable.

5.2. *Interpretation of stable isotopes and trace metals*

5.2.1. *$\delta^{18}O$ profile*

Monitoring data from Ejulve cave demonstrate that the $\delta^{18}O$ signal of modern calcite reflects the $\delta^{18}O$ value of the dripwater, which is controlled mainly by the surface air temperature (Pérez-Mejías et al., 2018). On a seasonal scale, previous $\delta^{18}O$ monitoring data obtained from farmed calcite do not show a clear pattern, probably due to the combination of other factors such as the source of moisture (i.e. synoptic patterns of the rainfall and the air mass history) which was suggested as additional control together with surface air temperature (Pérez-Mejías et al., 2018). On longer timescales, a previous speleothem record from this cave covering past glacial-interglacial transitions, suggests a source effect on the $\delta^{18}O$ speleothem composition during short events at the end of the Termination III via the influence of major freshwater pulses into the North Atlantic (Pérez-Mejías et al., 2017).

Several factors influenced the $\delta^{18}O$ values of ANDROMEDA. The record may be split into two parts, the first one spanning from 119 to 80 kyr, and the second part from 80 to 36 kyr, with a transition period between 80 and 65 kyr (Fig. 6). During MIS 5, $\delta^{18}O$ follows the precessional cycle of the boreal summer, i.e. a higher ratio of Northern Hemisphere Summer Insolation (NHSI) promotes higher evaporation in the North Atlantic, providing more moisture to the Westerlies (Stoll et al., 2013). The increase in seasonal precipitation on the IP due to enhanced moisture delivery might explain the precession-paced $\delta^{18}O$ data of ANDROMEDA from 119 to 80 kyr, with lower $\delta^{18}O$ values pointing towards humid conditions. Lower precession, with boreal summer in perihelion, promotes drier summers/wetter winters (and thus, higher seasonality) on the IP which is consistent with the lowest $\delta^{18}O$ values recorded by the stalagmite prior to the peak of low precession (Fig. 6c and d). An increase in annual precipitation is in agreement with enhanced tufa

Table 1
^{230}Th dating results. The error is 2σ. Sample numbers refers to distance in mm from base.

Sample	^{238}U	^{232}Th	^{230}Th/^{232}Th	δ^{234}U[a]	^{230}Th/^{238}U	^{230}Th Age (yr)	$\delta^{234}U_{Initial}$[b]	^{230}Th Age (yr BP)[c]
Name	(ppb)	(ppt)	(atomic x10^{-6})	(measured)	(activity)	(uncorrected)	(corrected)	(corrected)
AND-12	73.4 ± 0.1	2443 ± 49	576 ± 12	421.3 ± 1.6	1.1626 ± 0.0020	161424 ± 723	663 ± 3	160776 ± 829
AND-40	160.4 ± 0.2	573 ± 12	4533 ± 91	415.2 ± 1.7	0.9825 ± 0.0018	119064 ± 458	581 ± 2	118934 ± 460
AND-58	191 ± 0	706 ± 14	4479.6 ± 90.1	491.2 ± 1.6	1.0021 ± 0.0020	111829 ± 421	673 ± 2	111700 ± 423
AND-89	171 ± 0.2	234 ± 5	11183 ± 226	414.3 ± 1.8	0.9269 ± 0.0019	108259 ± 433	562 ± 3	108169 ± 433
AND-125	192.6 ± 0.2	308 ± 6	9337 ± 189	446.2 ± 1.8	0.9057 ± 0.0019	100425 ± 382	592 ± 2	100332 ± 383
AND-130	173.9 ± 0.2	435 ± 9	5978 ± 120	455.3 ± 1.4	0.9071 ± 0.0011	99611 ± 249	603 ± 2	99497 ± 251
AND-135	186.3 ± 0.2	889 ± 18	3435 ± 69	580.0 ± 1.8	0.9941 ± 0.0020	100008 ± 365	769 ± 3	99865 ± 369
AND-140	157.4 ± 0.1	750 ± 15	3273 ± 66	536 ± 1.4	0.9457 ± 0.0011	97084 ± 225	705 ± 2	96935 ± 232
AND-144	140 ± 0	1003 ± 20	2151.2 ± 43.3	587.4 ± 2.0	0.9376 ± 0.0018	90897 ± 306	759 ± 3	90714 ± 317
AND-154	125 ± 0	563 ± 11	3436.1 ± 69.1	720.9 ± 1.8	0.9421 ± 0.0016	80905 ± 234	906 ± 2	80772 ± 238
AND-170	122 ± 0.1	205 ± 4	8581 ± 173	606 ± 1.3	0.8724 ± 0.0010	80516 ± 163	761 ± 2	80420 ± 164
AND-185	143.5 ± 0.1	193 ± 4	11320 ± 229	708.2 ± 1.4	0.9214 ± 0.0011	79299 ± 159	886 ± 2	79210 ± 160
AND-205	133 ± 0.1	178 ± 4	10697 ± 217	671.7 ± 1.4	0.8690 ± 0.0011	75486 ± 156	831 ± 2	75397 ± 157
AND-220	151 ± 0	200 ± 4	9365.4 ± 189.3	440.2 ± 1.6	0.7486 ± 0.0015	76463 ± 249	546 ± 2	76374 ± 250
AND-230	165 ± 0.2	286 ± 6	7731 ± 156	617.1 ± 2.0	0.8124 ± 0.0017	72246 ± 238	757 ± 3	72153 ± 239
AND-240	142 ± 0.2	195 ± 4	9778 ± 198	754.4 ± 2.0	0.8162 ± 0.0017	64867 ± 200	906 ± 2	64782 ± 200
AND-248	95 ± 0	327 ± 7	3080.8 ± 62.3	504.9 ± 1.8	0.6404 ± 0.0014	58384 ± 185	595 ± 2	58257 ± 190
AND-271	121.5 ± 0.2	163 ± 3	7796 ± 158	636.8 ± 1.9	0.6333 ± 0.0013	51531 ± 155	736 ± 2	51444 ± 155
AND-300	134.7 ± 0.1	200 ± 4	6150 ± 125	494.2 ± 1.8	0.5533 ± 0.0010	49051 ± 136	568 ± 2	48960 ± 137
AND-309	132.7 ± 0.1	131 ± 3	9577 ± 195	636.9 ± 1.8	0.5751 ± 0.0012	45806 ± 135	725 ± 2	45725 ± 136
AND-318	119.1 ± 0.1	78 ± 2	14428 ± 296	650.9 ± 1.9	0.5738 ± 0.0011	45187 ± 127	739 ± 2	45112 ± 127
AND-338	69.1 ± 0.1	187 ± 4	3371 ± 69	884.1 ± 2.0	0.5546 ± 0.0013	36960 ± 109	981 ± 2	36856 ± 112
AND-349	82 ± 0	150 ± 3	2366.5 ± 48.4	1171.2 ± 2.0	0.2636 ± 0.0007	13955 ± 40	1218 ± 2	13867 ± 44
AND-390	51 ± 0	611 ± 12	240.4 ± 4.9	799.1 ± 1.8	0.1753 ± 0.0008	11096 ± 52	824 ± 2	10840 ± 145
AND-400	246 ± 0	571 ± 11	601.6 ± 12.3	826.2 ± 2.1	0.0847 ± 0.0004	5164 ± 23	838 ± 2	5064 ± 35
AND-410	168.8 ± 0.2	194 ± 4	1169 ± 24	807.3 ± 2.0	0.0816 ± 0.0003	5019 ± 19	819 ± 2	4936 ± 23

Corrected ^{230}Th ages assume the initial ^{230}Th/^{232}Th atomic ratio of $4.4 \pm 2.2 \times 10^{-6}$. Those are the values for a material at secular equilibrium, with the bulk earth ^{232}Th/^{238}U value of 3.8. The errors are arbitrarily assumed to be 50%.
[a] $\delta^{234}U = ([^{234}U/^{238}U]_{activity} - 1)x1000$.
[b] $\delta^{234}U_{initial}$ was calculated based on the ^{230}Th age (T), i.e., $\delta^{234}U_{initial} = \delta^{234}U_{measured}$ x $e^{\lambda 234xT}$.
[c] B.P. stands for "Before Present" where the "Present" is defined as the year 1950 A.D.

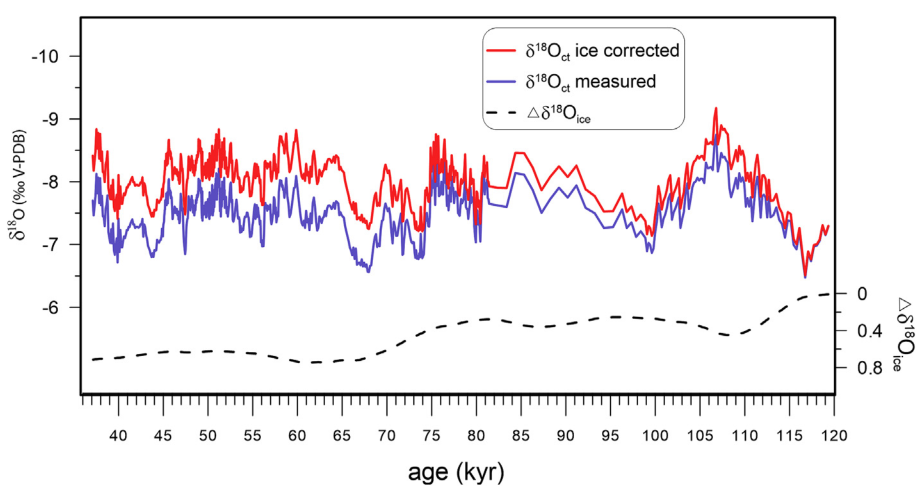

Fig. 4. δ^{18}O record of ANDROMEDA corrected for the global ice-volume effect following Bintanja et al. (2005).

deposition in NE Iberia at that time (Sancho et al., 2015).

At ~80 kyr, a trend of decreasing relative sea level (RSL) (Grant et al., 2014) and colder sea-surface temperatures (SST) (Martrat et al., 2014) in the IM and cold conditions in Greenland (Fig. 6j, a, k) mark the transition to MIS 4. The onset of cold conditions imprinted a millennial-scale variability superimposed on the long-term δ^{18}O-precession trend (Fig. 6c and d) via a reduction of sea surface evaporation and a concomitant decrease of moisture delivery towards Europe. During the transition between the two phases seen in the stalagmite around ~80-65 kyr (onset of HS-6), δ^{18}O variability does not coincide exactly with the peak of low precession, although the long-term δ^{18}O-precession trend is still noticeable. In that way, an imprint of the temperature effect on the δ^{18}O values of the stalagmite should not be discarded. Lower stalagmite δ^{18}O values would imply more humid but also colder conditions, in concordance with a trend towards cold temperatures in Greenland and low SST in the Atlantic Ocean (Fig. 6c, k, a). This hypothesis is supported by the lack of evidence of paleoglaciers retreat in northern Iberia (Rodríguez-Rodríguez et al., 2016; Sancho et al., 2018) suggesting a cold but relatively humid climate (Moreno et al., 2012).

Subsequent to ~65-60 kyr, coincident with HS-6, the δ^{18}O and δ^{13}C values of ANDROMEDA start to co-vary (Fig. 6c, e) suggesting that for the first time in this record, both isotopes responded to the

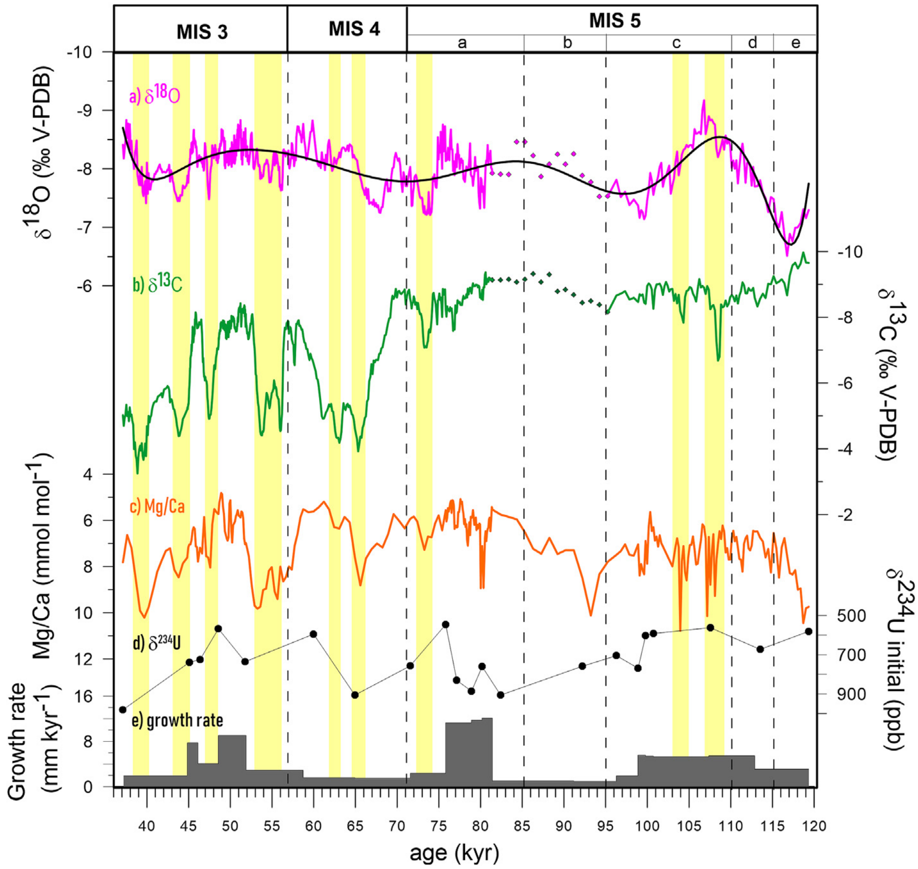

Fig. 5. ANDROMEDA proxy record. From top to bottom: a) $\delta^{18}O$ corrected for changes in global ice volume (pink), polynomial fit (black), b) $\delta^{13}C$ (green), c) Mg/Ca (orange), d) $\delta^{234}U$ initial (grey) and e) growth rate. The vertical yellow bars mark maxima of both $\delta^{13}C$ and Mg/Ca. (For interpretation of the references to color in this figure legend, the reader is referred to the Web version of this article.)

same process(es) such as changes in precipitation (see below). During this stage $\delta^{18}O$ shows a lag with respect to the precession of the boreal summer, in a period characterized by weak precession amplitude and low sea level (Fig. 6).

5.2.2. *$\delta^{13}C$ and Mg/Ca*

The $\delta^{13}C$ data are discussed separately for the two parts of the record. In the first part, spanning mostly MIS 5, $\delta^{13}C$ data are stable with the lowest values of the entire record and a small variability. During MIS 5, the lower $\delta^{13}C$ values range between −10 and −9‰ and the higher values between −9 to −8‰, slightly lower than the values reached during the Holocene in the top part of ANDROMEDA and similar to $\delta^{13}C$ values of a stalagmite which grew during the mid-to-late Holocene in this cave (Moreno et al., 2017).

The $\delta^{13}C$ values of ANDROMEDA reflect vegetation productivity and soil activity, i.e. lower $\delta^{13}C$ values are controlled by biogenic CO_2 of plant root respiration and soil microbial activity. This interpretation is supported by the present-day cave dynamics, when lower $\delta^{13}C$ values in the farmed calcite occur during the seasons of effective precipitation (Pérez-Mejías et al., 2018). The sensitivity to hydrological changes is also supported by the strong correlation between $\delta^{13}C$ and Mg/Ca. Prior calcite precipitation (PCP) leads to higher values of Mg/Ca, as the distribution coefficient of the Mg is much less than one, resulting in a larger reduction in Ca and increasing the Mg/Ca ratio in solution (Fairchild and Treble, 2009). PCP implies degassing of CO_2, a process that results in a systematic rise in $\delta^{13}C$. Therefore, the correlation between $\delta^{13}C$ and Mg/Ca suggests a hydrologic control on $\delta^{13}C$. This is also supported by the coincidence of high $\delta^{13}C$ with high values of $\delta^{234}U$ despite the limited resolution of the latter (Fig. 5d). $\delta^{234}U$ reflects the seepage water from which it formed, so its variability has been recognized as a proxy of the water residence time in the epikarst (Hellstrom and McCulloch, 2000; Polyak et al., 2012).

The larger basal diameter of ANDROMEDA along with the $\delta^{18}O$ and $\delta^{13}C$ values suggests the wettest period of the record during MIS 5, resulting in higher water availability supporting a well-developed Mediterranean vegetation cover. Together with the hydrological availability, temperature is the other major factor controlling vegetation activity. During MIS 5, the $\delta^{13}C$ record mimics the SST evolution in the IM and exhibits sensitivity to short cold events such as C23 and C24 (Fig. 6a, e). Although a decrease in the production of biogenic CO_2 during cold-dry episodes of MIS 5 is not ruled out, the high resilience of the Mediterranean vegetation (Aranbarri et al., 2014) could explain the small $\delta^{13}C$ variability and the fast return to low values during episodes of abrupt changes such as MIS 5c (Fig. 5b). This interpretation is in full accordance with the development of Mediterranean forests below 40 °N, controlled by the precessional cycle of boreal summer with short periods of contraction during the C27 to C24 cold marine periods. The latter were associated with the reduction in moisture availability as a response to changes in the North Atlantic (Tzedakis, 2005; Fletcher and Sánchez-Goñi, 2008; Sánchez-Goñi et al., 2008).

The cold temperatures in Greenland and in the IM after ~70 kyr (Fig. 6g, a) may be responsible for a decrease in the vegetation cover leading to higher $\delta^{13}C$ values in the stalagmite. Around 68 kyr, the $\delta^{13}C$ profile reach the highest values not seen previously in the

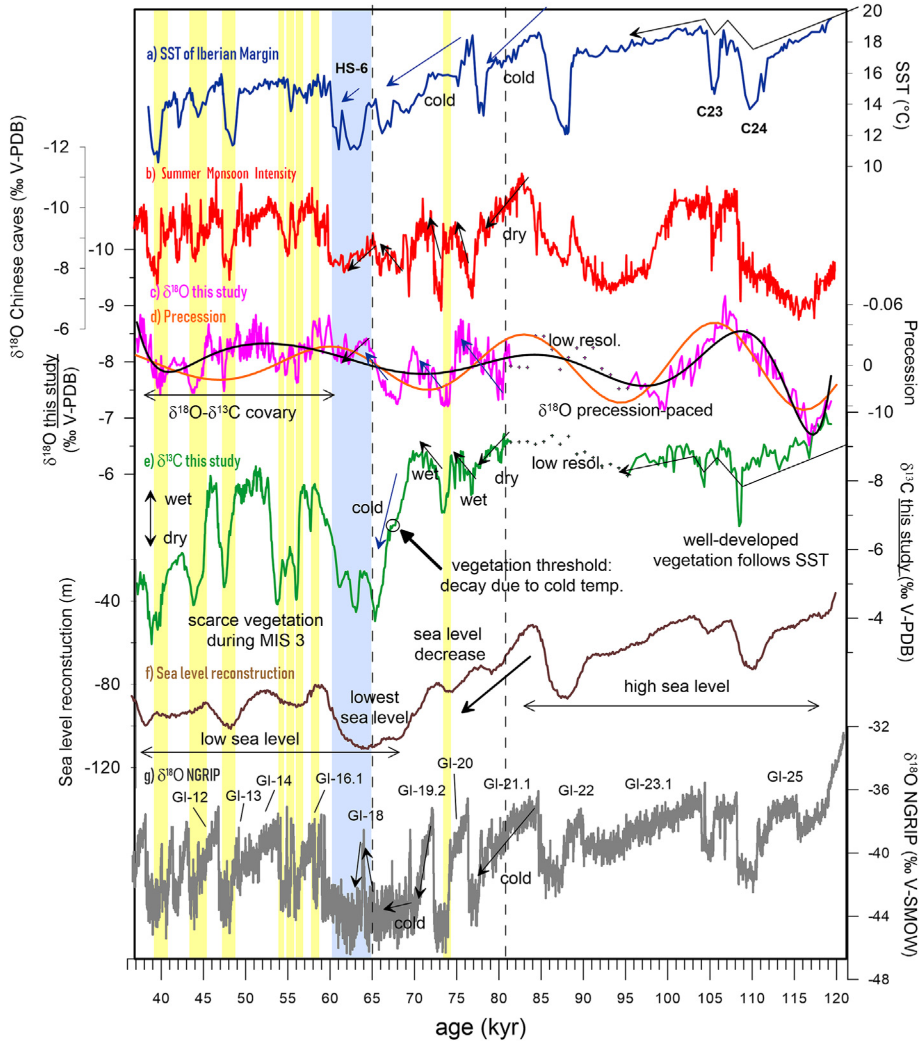

Fig. 6. Interpretation of the isotope variability of the ANDROMEDA record. From top to bottom: a) SST on the Iberian Margin (blue) (Martrat et al., 2007), b) $\delta^{18}O$ of the composite of Chinese caves (red) (Cheng et al., 2016), c) $\delta^{18}O$ of ANDROMEDA (this study) (pink) and polynomial fit (black), d) precessional cycle of boreal summer (orange) (Laskar et al., 2004), e) $\delta^{13}C$ of ANDROMEDA (this study) (green), f) relative sea-level (brown) (Grant et al., 2014) and g) $\delta^{18}O$ of NGRIP (North Greenland Ice Core Project members, 2004) with some GI remarked following Rasmussen et al. (2014). The NGRIP age model has been converted to years BP for comparison with other records. The vertical yellow bars show the high values of both $\delta^{18}O$ and $\delta^{13}C$ in our record, reflecting cold-dry periods. The vertical black dashed lines reflect two different stages and the transition between them, attending to the mechanisms controlling the climate. HS-6 is also marked with a blue bar. The arrows show the trends and similarities between records. The section with the lowest resolution in our isotope record is marked by dots. The nomenclature of C events follows Rousseau et al. (2006). (For interpretation of the references to color in this figure legend, the reader is referred to the Web version of this article.)

ANDROMEDA record, suggesting that a threshold has been overcome in the vegetation due to the cold-dry conditions (Fig. 6e).

In the second part of the record, the high variability in $\delta^{13}C$ and the covariation with $\delta^{18}O$ ($\rho = 0.53$, p-value < 0.001, $n = 500$) suggest a common response to a decrease in precipitation. As a consequence, higher $\delta^{13}C$ and $\delta^{18}O$ values were recorded during the cold spells of HS associated with dryness, while lower $\delta^{13}C$ and $\delta^{18}O$ were recorded during warm and humid interstadials, in agreement with pollen data (Combourieu Nebout et al., 2002; Sánchez-Goñi et al., 2002). Low $\delta^{13}C$ values are reached during humid periods reflecting enhanced soil biogenic productivity and more water availability, while higher $\delta^{13}C$ values during MIS 4-3 (−6.62‰) compared with MIS 5 (−8.59‰) suggest lower soil bioproductivity, less water availability and the prevalence of steppic taxa during this period, consistent with paleovegetation data (Combourieu Nebout et al., 2002; Vegas et al., 2010).

5.3. Last interglacial and glacial inception

5.3.1. Orbital control and abrupt dry-cold events

During the first (older) precession cycle of boreal summer insolation (~120-95 kyr), the $\delta^{18}O$ values of ANDROMEDA follow closely the orbital forcing (Fig. 7d and e). Precession-driven changes in precipitation have been described from regions affected by changes in the position of the Intertropical Convergence Zone such as the Middle East (Bar-Matthews et al., 2003) and the Asian Summer Monsoon (ASM) region of SE China (Cheng et al., 2016). Close to the subtropical band, some Mediterranean records exhibit seasonality related to precession (Regattieri et al., 2015; Roberts et al., 2008; Toucanne et al., 2015). In the regional context of the IP, ANDROMEDA and another speleothem record from northern Iberia (Stoll et al., 2015) also present a precession path in the $\delta^{18}O$ data. This could suggest a precession modulation in the intensity of the storm tracks associated to the Westerlies or alternatively an $\delta^{18}O$ imprint on the speleothems from northern Iberia by moisture

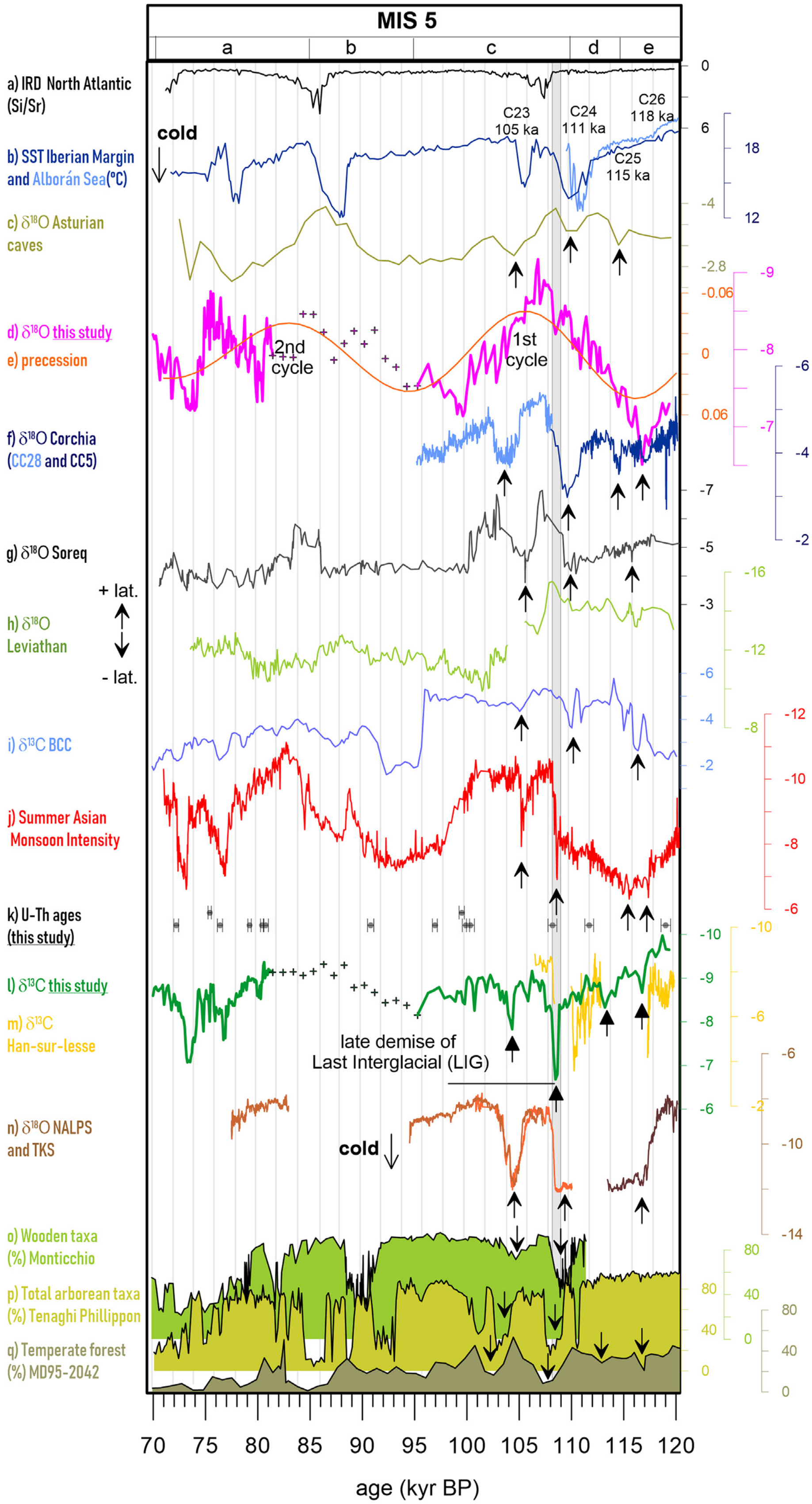

Fig. 7. Comparison of records during MIS 5, including orbital forcing. From top to bottom: a) IRD discharge at U1308 (Si/Sr) (black) (Hodell et al., 2008), b) SST at MD01-2444 on the Iberian Margin (blue) (Martrat et al., 2007) and at ODP-976 in the Alborán Sea (sky blue) (Martrat et al., 2014) where the C events has also been noted (Oppo et al., 2006), c) $\delta^{18}O$ of Asturias Caves (Stoll et al., 2015), δ) $\delta^{18}O$ of ANDROMEDA (pink) and e) precessional cycle of boreal summer (orange) (Laskar et al., 2004), f) $\delta^{18}O$ of Corchia Cave, Northern Italy

derived from the tropics.

The orbital pacing of $\delta^{18}O$ of ANDROMEDA is also noticeable during the second cycle of precession of boreal summer (Fig. 7d and e). Afterwards, $\delta^{18}O$ exhibits a saw-tooth pattern, suggesting a millennial-scale variability superimposed on the long-term orbital pacing, while $\delta^{13}C$ shows low values during the peak of low precession.

This long-term pattern in the $\delta^{18}O$ record was overprinted by abrupt events of higher values associated with millennial-scale cooling of SST in the IM caused by AMOC weakening events (Fig. 7a and b). These events are better expressed in the $\delta^{13}C$ record, where four maxima appear, the strongest at 108.5 and 104.3 kyr, and the weakest at 117 and 113 kyr (black arrows in Fig. 7l). These events coincided with cold events identified by temperature-sensitive speleothems in the Alps (Meyer et al., 2008; Boch et al., 2011) (Fig. 7b, l, n). The tight relationship between $\delta^{13}C$ and temperature in this interval implies an inherent temperature sensitivity of the $\delta^{13}C$ signal recorded by ANDROMEDA that also responds to changes in hydrology (see section 5.2.2).

The four events of high $\delta^{13}C$ values occurred during a decline of temperate forests as recorded by pollen data from the IM (Sánchez-Goñi et al., 2008) (Fig. 7q). Those events are clearly expressed in the marine record (C26 to C23) but generally only the two more intense ones (C24 and C23) are reflected in continental sequences, such as the pollen records from Lago Grande di Monticchio and Tenaghi Philippon (Martin-Puertas et al., 2014; Wulf et al., 2018) (Fig. 7o, p). The sensitivity of records from Southern Europe to changes in the North Atlantic during MIS 5 has been recently supported by the findings of Tzedakis et al. (2018) linking North Atlantic cold events and southern European aridity events in a marine core from the IM.

The two older and weaker events detected in the ANDROMEDA $\delta^{13}C$ record could be contemporary to the marine C26 and C25 events (Fig. 7b, l), barely evident in SST proxies in the Alborán Sea and on the IM, but showing that the interglacial was coming to an end after 115 kyr (Martrat et al., 2014). The cold-dry excursion at 117 kyr, analogue of C26 in ANDROMEDA, is seen in many records worldwide, with a weaker Asian monsoon (Fig. 7j), lower temperatures recorded by Alpine speleothems (Meyer et al., 2008), a drop in $\delta^{13}C$ in Belgian (Fig. 7m, n) and Hungarian speleothems (Demény et al., 2017), and the lowest growth rate in Lebanon speleothems (Nehme et al., 2015). In contrast to C26, the C25 event (113 kyr) is not recorded globally and is absent in both North America (Lachniet et al., 2014; Springer et al., 2014) and Israel (Bar-Matthews et al., 2003), as well in East Asia (Cheng et al., 2016) (Fig. 7h, i, j). The muted response in Corchia and Asturian caves (Drysdale et al., 2007; Stoll et al., 2015; Tzedakis et al., 2018) to C25 (Fig. 7c, f) suggests a common response in south-western Europe, although more data in other areas are needed to better understand the regional impact of this event.

The most pronounced $\delta^{13}C$ events of our record during this period are certainly those coinciding with the C24 and C23, well known and well expressed events worldwide (Fig. 7). Around 110.5 kyr, the C24 event is manifested by a drop from 18 °C to 13 °C in the SST on the IM, pointing to the end of the LIG in the North Atlantic covered seasonally by sea ice (Martrat et al., 2007). In this state, the AMOC is expected to be subject to rapid instabilities leading to sub-millennial variability (Capron et al., 2010). The increase in the size of the polar ice sheets makes them more vulnerable to perturbations than the large polar ice sheet of MIS 4 and 3 (Capron et al., 2010). The strong NHSI and the discharge of meltwater during IRD events could have been of enough magnitude to produce a change in the state of the AMOC. The C24 event is represented in ANDROMEDA by the highest $\delta^{13}C$ values of the MIS 5, and dated at 108.6 ± 0.3 kyr, in agreement with other absolute chronologies, e.g. the NALPS record (Fig. 7j, l, n). Lastly, the C23 (105 kyr) event was also identified globally in North Hemisphere records with the exception of Leviathan cave, that recorded a hiatus at that time (Fig. 7h).

5.3.2. The end of the last interglacial

The timing of the end of the Eemian interglacial forests in Europe is still controversially discussed (Sánchez-Goñi et al., 2005; Müller and Sánchez-Goñi, 2007; Brewer et al., 2008), but there is general agreement in the relative timing of records from similar latitudes. The varve-counted Eifel maar record established a similar chronology for the end of the Eemian (118 kyr - Sirocko et al., 2005) as a speleothem record from Belgium (117.3 kyr - Vansteenberge et al., 2016) (Fig. 7m). Speleothems from southern Iberia (~111 kyr - Hodge et al., 2008), Mallorca (111.7 ± 0.2 to 109.3 ± 0.2 kyr - Dumitru et al., 2018), northern Iberia (~112 kyr - Rossi et al., 2014) and Corchia cave, Italy (112.0 ± 0.8 to 108 ± 0.8 kyr - Drysdale et al., 2007) indicate a later demise of the LIG. A later chronology is suggested by a pollen record from the IM that exhibits a tie-point of non-arboreal peak abundance around ~107 kyr (Sánchez-Goñi et al., 2005; Müller and Sánchez-Goñi, 2007). This age is in line with an independent chronology for the LIG based on tephra layers in Lago Grande di Monticchio (40°57′N) (107.6–109.5 kyr - Allen and Huntley, 2009; Martin-Puertas et al., 2014), and Tenaghi Philippon (40°58′N) (109.4 ± 0.9 kyr - Wulf et al., 2018) (Fig. 7o,p). Both pollen records, similar in latitude to Ejulve cave (40°45′N), match our date of 108.6 ± 0.3 kyr for the major aridity event seen in $\delta^{13}C$ that could be attributed to the end of the LIG in this area.

5.4. Abrupt millennial-scale variability during MIS 4 to MIS 3

5.4.1. D-O variability

The Last Glacial cycle was characterized by a great expansion of high-latitude ice sheets involving widespread global impacts (Clark et al., 2009). In this context, the occurrence of D-O oscillations was the most notable expression of abrupt millennial-scale variability. The identification of the terrestrial response to D-O events in Villars cave (Genty et al., 2003, 2010) was a milestone to constrain the impact of those events in Europe. Subsequent studies have shown that the proxy signal of D-O events recorded by stalagmites differ across Europe. For instance, Sofular Cave located in northern Turkey exhibits a high sensitivity to D-O cycles (Fig. 8h) similar to the NGRIP ice core record (Fig. 8m), while Soreq cave lacks a clear response (Fig. 8f). Recently, speleothems from Crag Cave revealed short pulses of carbonate deposition during the Greenland Interstadials (GI) of the younger part of MIS 3 (GI-1 through to GI-3)

(navy blue) (Drysdale et al., 2007; Tzedakis et al., 2018), g) $\delta^{18}O$ of Soreq Cave, Israel (black) (Bar-Matthews et al., 2003), h) $\delta^{18}O$ of Leviathan Cave, Western USA (green) (Lachniet et al., 2014), i) $\delta^{13}C$ of BCC Cave, eastern USA (blue) (Springer et al., 2014), j) $\delta^{18}O$ of Chinese Caves (red) (Cheng et al., 2016), k) U-Th ages of ANDROMEDA, l) $\delta^{13}C$ of ANDROMEDA (green), m) $\delta^{13}C$ of Han-sur-lesse, Belgium (yellow) (Vansteenberge et al., 2016), n) $\delta^{18}O$ of Entrische Kirche cave, Austria (dark brown) (Meyer et al., 2008) and NALPS stalagmites (light brown) (Boch et al., 2011), o), woody taxa (%) in Lago Grande di Monticchio, southern Italy (green) (Martin-Puertas et al., 2014), p) total arborean taxa (%) (Wulf et al., 2018) (yellow) in Tenaghi Philippon, Greece, q) temperate forest (%) of MD95-2042 (khaki) (Sánchez-Goñi et al., 2017). Note that the isotope proxies of all stalagmite records are interpreted to reflect the amount of precipitation, with the exception of Leviathan (changes in moisture source), Han-sur-lesse (changes in vegetation type), $\delta^{13}C$ of ANDROMEDA (this study) and NALPS stalagmites (temperature effect). All vertical axes of the speleothem records are reversed, with the exception of NALPS. The nomenclature of C events follows Rousseau et al. (2006). The age models of Corchia and Leviathan were converted to years BP for comparison with the other records. (For interpretation of the references to color in this figure legend, the reader is referred to the Web version of this article.)

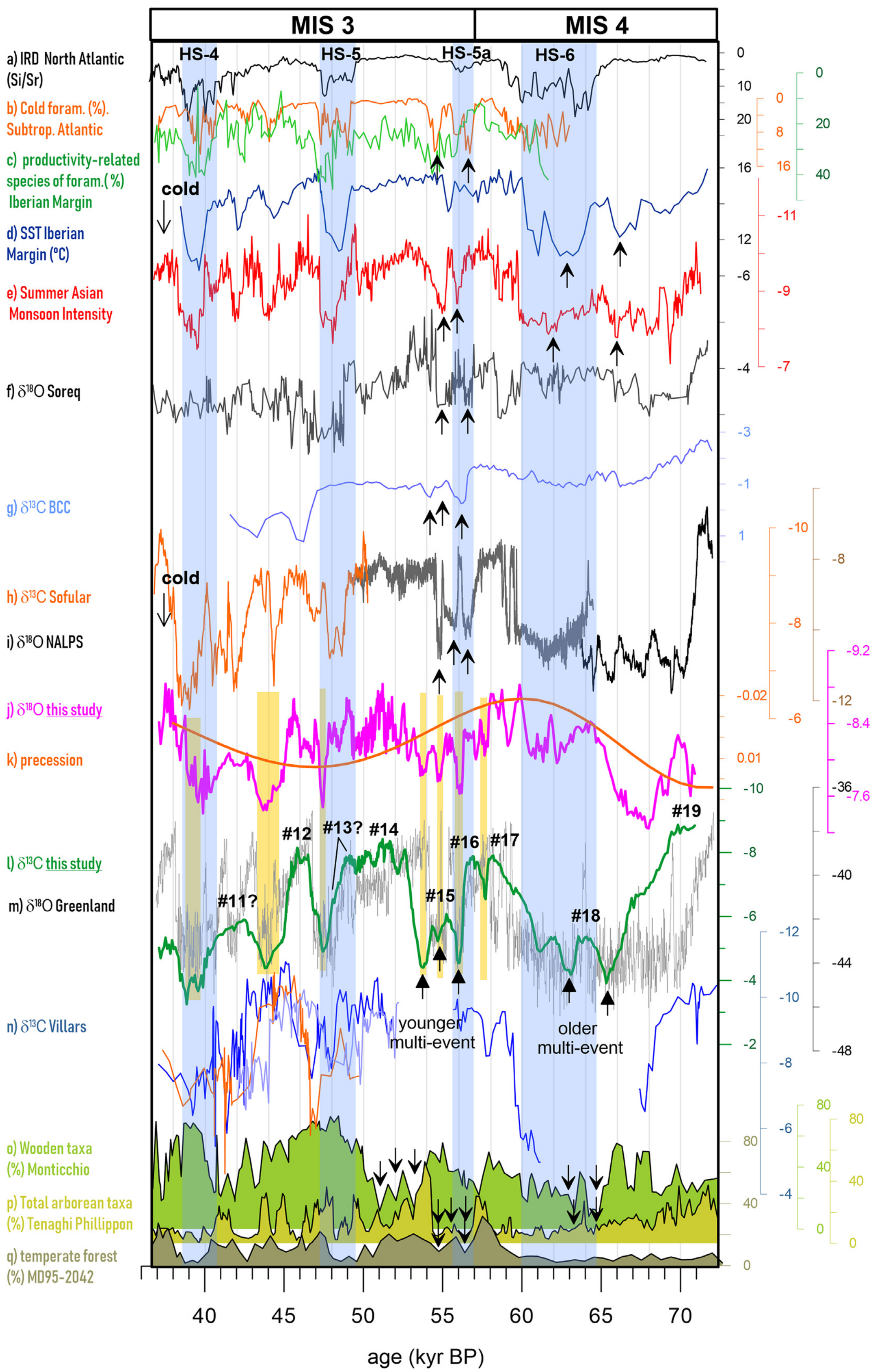

Fig. 8. Comparison of records during MIS 4 and 3, including orbital forcing. From top to bottom: a) IRD discharge at core site U1308 (Si/Sr) (black) (Hodell et al., 2008), b) cold-water foraminifera species (%) (*Neogloboquadrina pachyderma*, *Turborotalia quinqueloba*) in ODP 172–1060 (orange) (Vautravers et al., 2004), c) productivity-related species of planktic foraminifera (%) of MD01-2444 (*Globigerina bulloides*, *Globigerinita glutinata*) (green) (Vautravers and Shackleton, 2006), d) SST in MD01-2444 on the Iberian Margin (blue) (Martrat et al., 2007), e) δ^{18}O of Chinese speleothems (red) (Cheng et al., 2016), f) δ^{18}O of Soreq Cave (black) (Bar-Matthews et al., 2003), g) δ^{13}C of BCC Cave (blue) (Springer et al., 2014), h)

(Fankhauser et al., 2016), while a speleothem from Bunker Cave recorded growth during the warm conditions of D-O 14 and 12 (Weber et al., 2018) in agreement with previous records from Alps (Moseley et al., 2014). Besides, a speleothem from Cueva Victoria (southeast Iberia) shows the response to D-O oscillations associated with humid conditions (Budsky et al., 2019).

The ANDROMEDA $\delta^{13}C$ record, whose timing agrees with the NGRIP record for D-O 18 to 12 (Fig. 8l,m), replicates the signal seen in Villars cave and covers previous hiatuses during cold periods (Fig. 8l,n). Both $\delta^{13}C$ profiles from Villars and Ejulve exhibit a similar variability (~5‰) with ANDROMEDA recording generally higher values. D-O events 19 (~70 kyr) to D-O 11 (~42 kyr) are recorded by the ANDROMEDA record, while the identification of D-O 13, possibly because of its weak signal and short duration (Wainer et al., 2009), is uncertain. Likewise, the slow growth and the uncertainties of the age model challenge the identification of D-O 11.

5.4.2. Heinrich stadial variability

In modern summers, the Polar Front (PF) follows the coast of Greenland with a sinuous circulation (Dickson et al., 1988), while during HS its position was south of the Ruddiman IRD belt (Fig. 1), that reached as far as 39° N (Voelker and Abreu, 2011) or 40° N (Eynaud et al., 2009 and references therein). Naughton et al. (2009) proposed even lower latitudes for the PF for the maximum discharge phase of IRD during the HS, reaching as far as 35–37° N. The southward migration of the PF and the meridional compression of the North Atlantic anticyclonic gyre were the result of an enhanced zonal atmospheric circulation (Pailler and Bard, 2002) (Fig. 1). The suppression of the cyclogenesis, controlled by the low SST in the North Atlantic Ocean and an extensive winter ice cover, gave rise to reduced evaporation and a weakening of the AMOC (Genty et al., 2010; Rowe et al., 2012) which resulted in a dry and cold climate in Europe, explaining the hiatuses in some continental paleorecords (e.g. Villars cave, Han-Sur-Lesse, NALPS, Figs. 7m, n, 8n).

During such cold periods Ejulve cave at 40° N of latitude was likely located along the pathway of the storm tracks, when the PF and the Westerlies were displaced southward (Fig. 1). This may explain speleothem growth in Ejulve cave during HS, especially during HS-6. However, each cave system is unique and the latitudinal location below 40° N does not guarantee continuous growth during these periods, as was seen in speleothems from Portugal and Mallorca (Denniston et al., 2018; Dumitru et al., 2018).

The Heinrich stadials in ANDROMEDA are represented by high $\delta^{13}C$ values, although the absolute values differ between stadials. The corresponding HS-SST cooling phases are attributed to the slowdown of the AMOC and the related reduction in northward heat transport (McManus et al., 2004; de Vernal et al., 2006; Clement and Peterson, 2008; Wolff et al., 2010). In our record, HS-4 shows the highest $\delta^{13}C$ values, a Heinrich event associated with one of the most pronounced IRD fluxes of the last glacial period (Cortijo et al., 1997; Hemming, 2004) with a probably nearly complete shutdown of the thermohaline circulation (Elliot et al., 2002; Roche et al., 2004). Extremely dry conditions in Iberia during HS-4 were inferred by other proxies such as dust transported to the Alborán Sea (Moreno et al., 2002), paleovegetation data from southern Iberia (Sánchez-Goñi et al., 2002) and more recently by a loess sequence from central Iberia (Wolf et al., 2018). This accumulation of loess occurred in two phases, the first between 73.0 ± 6.9 kyr and 59.7 ± 4.7 kyr (matching HS-6) and the second between 41.3 ± 4.0 kyr and 43 ± 3.8 kyr, including HS-4 within dating uncertainties (Wolf et al., 2018).

5.4.3. Extreme multi-events complexes

A prominent feature between 70 and 50 kyr in the $\delta^{13}C$ record of ANDROMEDA are two extreme multi-events, characterized by their high $\delta^{13}C$ values with a brief interval in between resulting in a W-shape pattern (dubbed multi-event, Fig. 8l). The first of these events incorporates HS-6 and D-O 18, and the second multi-event comprises HS-5a and D-O 15. The $\delta^{13}C$ record shows comparable values for both multi-events but of different length, the older multi-event being the longer one. These events coincide with IRD discharge, increases in the abundance of cold taxa foraminifera *(N. pachyderma, T. quinqueloba)* and/or productivity-related species (*G. bulloides, G. glutinata*) (Fig. 8a,b,c). Interestingly, both multi-events correspond to hiatuses in the Villars cave record (Fig. 8n) and coincide with a common decrease in arborean pollen in the European records (Fig. 8o,p,q), supporting the persistence of markedly dry conditions.

During the older multi-event (including HS-6 and D-O 18), the $\delta^{13}C$ record of ANDROMEDA exhibits a similar pattern as the SST of the IM (Fig. 8l,d). Mg/Ca data of ANDROMEDA reveal two phases: a first one with markedly dry conditions until 65.5 kyr, coincident with the highest values in $\delta^{13}C$, and a second phase of enhanced water availability from 65.5 kyr onwards, within HS-6 (Fig. 5c). The change from one to the other phase occurred during the interstadial D-O 18 around 64 kyr. Interestingly, the Mg/Ca results show that the driest conditions ocurred before HS-6, suggesting the influence of very cold conditions associated with MIS 4. Globally, only the $\delta^{18}O$ record of the East Asian Monsoon region exhibits a similar phasing to that seen in our $\delta^{13}C$ for this period (Fig. 8e,l). More speleothem records covering HS-6 are needed to clarify the climate mechanisms and timing during this multi-event.

The younger multi-event (including HS-5a and D-O 15) presents a different signal depending on the latitude in the marine realm (North Atlantic or subtropical Atlantic). Thus, only a brief reduction in the SST of the IM in an isolated event is observed during this time interval (Fig. 8d). Some authors suggested the existence of HS-5a at this time, an additional Heinrich event between HS-5 and HS-6 (e.g. Rashid et al., 2003; Vautravers and Shackleton, 2006) with low IRD deposition (Fig. 8a). However, the absence of major iceberg discharges into the North Atlantic and the lack of a marked decrease in SST of the IM are in contrast with the prominent increase in cold-water foraminifera recorded in the subtropical western Atlantic (Gulf Stream area) (Vautravers et al., 2004), suggesting sensitivity in lower latitudes to these changes. Likewise, the increase in productivity-related species of planktic foraminifera, a proxy of upwelling particularly in the northeastern subtropical Atlantic (Chapman et al., 1996; Vautravers and Shackleton, 2006), reflects an increase in trade wind intensity in this sector (Vautravers and Shackleton, 2006). The strengthening of trade winds is a consequence of a stronger Hadley Cell, reinforcing the subtropical highs and producing a northward displacement of the subtropical jet that could explain the dry conditions reflected by the pollen data in this period (Martin-Puertas et al., 2014; Sánchez-Goñi et al., 2017; Wulf et al., 2018) (Fig. 8o,p,q). The lack of planktonic data during the

$\delta^{13}C$ of Sofular Cave (blue) (Fleitmann et al., 2009), i) $\delta^{18}O$ of NALPS (grey) (Moseley et al., 2014), (black) (Boch et al., 2011), j) $\delta^{18}O$ of ANDROMEDA (pink) with a polynomial fit (black) and k) precessional cycle of boreal summer (orange) (Laskar et al., 2004), l) $\delta^{13}C$ of ANDROMEDA (green), m) $\delta^{18}O$ of NGRIP (North Greenland Ice Core Project members, 2004), n) $\delta^{13}C$ of Villars Cave (blue) (light blue) (orange) (Genty et al., 2010), o) woody taxa (%) of Monticchio (green) (Allen and Huntley, 2009), p) total arborean taxa (%) (Wulf et al., 2018) (yellow) in Tenaghi Philippon, temperate forest (%) of q) MD95-2042 (khaki) (Sánchez-Goñi et al., 2017). The vertical axes of the speleothem records are reversed, with the exception of NALPS. The NGRIP age model was converted to years BP for comparison with other records. (For interpretation of the references to color in this figure legend, the reader is referred to the Web version of this article.)

previous multi-event, together with previous considerations that HS-6 is poor in foraminifera species indicative of upwelling in the northeastern subtropical Atlantic (Vautravers and Shackleton, 2006) prevents at this time the consideration of that mechanism for the older multi-event. On the contrary, this mechanism could be applied also to events HS-5 and HS-4 that also display an increase in the productivity-related species (Fig. 8c).

The suggested mechanism shows similarities to the NAO index, but it is worth noting that the Northern Hemisphere ice sheets affected the strength and extent of the semi-permanent atmospheric activity centers, namely the Icelandic Low and the Azores High that control the NAO. Therefore, some authors that invoke similar mechanisms to explain past climate conditions refer to NAO + like conditions during stadials (Sánchez-Goñi et al., 2002) or during periods of enhanced upwelling in the IM (Vautravers and Shackleton, 2006), while Naughton et al. (2009) refer to the reminiscences of the present-day prevailing modes of the NAO to explain the climate variability during HS 4, 2 and 1.

Another particularity of this younger multi-event is that it started with a Heinrich stadial, in contrast to the older multi-event. Our data therefore record an abrupt response of the terrestrial realm, with Mg/Ca pointing towards dry conditions during the full duration of this multi-event (Fig. 5b and c), in contrast to the two-phases seen in the previous event. Additionally, the younger multi-event had a global impact in contrast to the older multi-event, with changes in the subtropical Atlantic that triggered cold-dry anomalies in North America (BCC cave) (Springer et al., 2014), Europe (NALPS, Ejulve cave) (Moseley et al., 2014) and Asia (Soreq) (Bar-Matthews et al., 2003) (Fig. 8h, j, n, f).

While the response of the vegetation to the older multi-event was contemporary to the response of $\delta^{13}C$ of ANDROMEDA, this was not the case for the younger multi-event. The comparison between the Monticchio pollen record and $\delta^{13}C$ of ANDROMEDA suggests a displacement towards younger ages in Monticchio during the younger multi-event by 3–4 kyr (black arrows, Fig. 8o). A similar shift is suggested for D-O 14, which shows an increase in wooden taxa during the HS-5. Previous studies pointed out discrepancies in the chronology of Monticchio during MIS 3, such as during HS-4, due to a poor varve preservation (Wulf et al., 2004). The results presented here suggest that the response to the multi-events could have been synchronous in both records.

To sum up, the older multi-event shows high IRD discharge and cold SSTs on the IM, and our data suggest that it consisted of two parts, i.e. a dry one until 65.5 kyr and more humid one afterwards. The dry phase reflects changes in the ocean-atmosphere system prior to HS-6. On the contrary, the younger multi-event shows a higher response in the subtropical Atlantic compared to the North Atlantic, with an increase in cold-water foraminifera and productivity-related species at lower latitudes. The increase in trade wind intensity and an intensified Hadley Cell could be responsible of a northward displacement of the Westerlies, and hence, gave rise to dry conditions in Iberia during this multi-event. Our results reinforce the consideration of drier conditions in the Mediterranean realm as a response of a colder North Atlantic.

6. Conclusions

The ANDROMEDA stalagmite from Ejulve cave grew continuously from 118.9 to 36.9 kyr. With respect to the $\delta^{18}O$ proxy data, we proposed two different stages: (1) during MIS 5, $\delta^{18}O$ was controlled by orbital pacing, with boreal summer precession minima leading to humid conditions, and (2) MIS 4 and 3, when $\delta^{18}O$ and $\delta^{13}C$ co-varied after HS-6 and the variability of both isotopes reflects a common response to reduced precipitation.

During the first stage (MIS 5), $\delta^{18}O$ was controlled by an increase in seasonality due to lower precession (boreal summer in perihelion), with more humid winters reflecting enhanced moisture transport by the Westerlies. The $\delta^{13}C$ data, highly correlated with Mg/Ca, record vegetation productivity, soil microbial activity and water availability. The dominant orbital pacing (precession) on $\delta^{18}O$ was interrupted by abrupt dry-cold periods. We found evidence of four such events which coincided with the C26, C25, C24 and C23 cold events in the North Atlantic. The end of the LIG in the study area occurred at 108.6 ± 0.3 kyr, in agreement with other records in southern Europe and supporting the hypothesis of a late demise in southern compared to central Europe.

During the second stage (MIS 4 and 3), $\delta^{18}O$ lagged the precession signal, and $\delta^{13}C$ reflects the succession of D-O and Heinrich events. These dry-cold periods are characterized by high values in both $\delta^{18}O$ and $\delta^{13}C$ due to a decrease in precipitation. The stalagmite's growth rate decreased during MIS 4 and the cold stages of MIS 3.

Two multi-events are recorded by $\delta^{13}C$ between 70 and 50 kyr, i.e., HS-6 and D-O 18 on the one hand, and HS-5a and D-O 18 on the other hand. Both multi-events show a similar intensity but a different duration, which was longer in the older multi-event. The latter is characterized by high IRD discharge in the North Atlantic and cold SST on the IM, and a dry climate until 65.5 kyr prior to HS-6 and more humid conditions afterwards in the study area. The younger multi-event shows a higher response in the subtropical Atlantic, with an increase in cold-water foraminifera and productivity-related species in lower latitudes. An intensified Hadley Cell and reinforced trade winds might have been responsible for a northward displacement of the subtropical jet and the Westerlies, giving rise to dry conditions in the study area.

Conflict of interest

No conflict of interest found.

Acknowledgements

We acknowledge the funding received from NSFC 41888101 and 41731174 to HC and NSF Grant 0172816 to RLE, the Government of Aragón predoctoral research grant B158/13 to CPM, CTM2013-48639-C2-2-R (OPERA); CTM2016-75411-R (CHIMERA) and CGL2016-77479-R (SPYRIT) projects to IC and AM respectively. We thank the Aragón Institute of Statistics for climatic datasets. We are also grateful to Yanbin Lu for his help in the U-Th laboratory in Minnesota, Joaquin Perona for stable isotope analyses (CCiT-UBCC), Paul Töchterle and Manuela Wimmer for useful advises during isotopic analysis (Innsbruck) and to all people who helped during field work and sampling in the IPE-CSIC lab. IC also thanks the ICREA Academia programme from the Generalitat de Catalunya.This article is dedicated to the memory of Professor Carlos Sancho.

References

Allen, J.R.M., Huntley, B., 2009. Last Interglacial palaeovegetation, palaeoenvironments and chronology: a new record from Lago Grande di Monticchio, southern Italy. Quat. Sci. Rev. 28, 1521–1538. https://doi.org/10.1016/j.quascirev.2009.02.013.

Aranbarri, J., González-Sampériz, P., Valero-Garcés, B., Moreno, A., Gil-Romera, G., Sevilla-Callejo, M., García-Prieto, E., Di Rita, F., Mata, M.P., Morellón, M., Magri, D., Rodríguez-Lázaro, J., Carrión, J.S., 2014. Rapid climatic changes and resilient vegetation during the Lateglacial and Holocene in a continental region of south-western Europe. Glob. Planet. Chang. 114, 50–65. https://doi.org/10.1016/j.gloplacha.2014.01.003.

Arienzo, M.M., Swart, P.K., Pourmand, A., Broad, K., Clement, A.C., Murphy, L.N., Vonhof, H.B., Kakuk, B., 2015. Bahamian speleothem reveals temperature decrease associated with Heinrich stadials. Earth Planet. Sci. Lett. 430, 377–386. https://doi.org/10.1016/j.epsl.2015.08.035.

Atsawawaranunt, K., Comas-Bru, L., Amirnezhad Mozhdehi, S., Deininger, M., Harrison, S.P., Baker, A., Boyd, M., Kaushal, N., Ahmad, S.M., Ait Brahim, Y., Arienzo, M., Bajo, P., Braun, K., Burstyn, Y., Chawchai, S., Duan, W., Hatvani, I.G., Hu, J., Kern, Z., Labuhn, I., Lachniet, M., Lechleitner, F.A., Lorrey, A., Pérez-Mejías, C., Pickering, R., Scroxton, N., SISAL Working Group Members, 2018. The SISAL database: a global resource to document oxygen and carbon isotope records from speleothems. Earth Syst. Sci. Data 10, 1687–1713. https://doi.org/10.5194/essd-10-1687-2018.

Bajo, P., Hellstrom, J., Frisia, S., Drysdale, R., Black, J., Woodhead, J., Borsato, A., Zanchetta, G., Wallace, M.W., Regattieri, E., Haese, R., 2016. "Cryptic" diagenesis and its implications for speleothem geochronologies. Quat. Sci. Rev. 148, 17–28. https://doi.org/10.1016/j.quascirev.2016.06.020.

Bar-Matthews, M., Ayalon, A., Gilmour, M.A., Matthews, A., Hawkesworth, C.J., 2003. Sea-land oxygen isotopic relationships from planktonic foraminifera and speleothems in the Eastern Mediterranean region and their implication for paleorainfall during interglacial intervals. Geochem. Cosmochim. Acta 67, 3181–3199.

Bintanja, R., van de Wal, R.S.W., Oerlemans, J., 2005. Modelled atmospheric temperatures and global sea levels over the past million years. Nature 437, 125–128. https://doi.org/10.1038/nature03975.

Boch, R., Cheng, H., Spötl, C., Edwards, R.L., Wang, X., Häuselmann, Ph., 2011. NALPS: a precisely dated European climate record 120–60 ka. Clim. Past 7, 1247–1259.

Brewer, S., Guiot, J., Sánchez-Goñi, M.F., Klotz, S., 2008. The climate in Europe during the Eemian: a multi-method approach using pollen data. Quat. Sci. Rev. 27, 2303–2315.

Budsky, A., Wassenburg, J.A., Mertz-Kraus, R., Spötl, C., Jochum, K.P., Gibert, L., Scholz, D., 2019. Western Mediterranean climate response to Dansgaard/Oeschger events - new insights from speleothem records. Geophys. Res. Lett. 2019GL084009 https://doi.org/10.1029/2019GL084009.

Capron, E., Landais, A., Chappellaz, J., Schilt, A., Buiron, D., Dahl-Jensen, D., Johnsen, S.J., Jouzel, J., Lemieux-Dudon, B., Loulergue, L., Leuenberger, M., Masson-Delmotte, V., Meyer, H., Oerter, H., Stenni, B., 2010. Millennial and sub-millennial scale climatic variations recorded in polar ice cores over the last glacial period. Clim. Past 6, 345–365. https://doi.org/10.5194/cp-6-345-2010.

Carolin, S.A., Cobb, K.M., Lynch-Stieglitz, J., Moerman, J.W., Partin, J.W., Lejau, S., Malang, J., Clark, B., Tuen, A.A., Adkins, J.F., 2016. Northern Borneo stalagmite records reveal West Pacific hydroclimate across MIS 5 and 6. Earth Planet. Sci. Lett. 439, 182–193. https://doi.org/10.1016/j.epsl.2016.01.028.

Chapman, M.R., Shackleton, N.J., Zhao, M., Eglinton, G., 1996. Faunal and alkenone reconstructions of subtropical North Atlantic surface hydrography and paleotemperature over the last 28 kyr. Paleoceanography 11, 343–357.

Cheng, H., Edwards, R.L., Sinha, A., Spötl, C., Yi, L., Chen, S., Kelly, M., Kathayat, G., Wang, X., Li, X., Kong, X., Wang, Y., Ning, Y., Zhang, H., 2016. The Asian monsoon over the past 640,000 years and ice age terminations. Nature 534, 640–646. https://doi.org/10.1038/nature18591.

Cheng, H., Lawrence Edwards, R., Shen, C.-C., Polyak, V.J., Asmerom, Y., Woodhead, J., Hellstrom, J., Wang, Y., Kong, X., Spötl, C., Wang, X., Calvin Alexander, E., 2013. Improvements in 230Th dating, 230Th and 234U half-life values, and U–Th isotopic measurements by multi-collector inductively coupled plasma mass spectrometry. Earth Planet. Sci. Lett. 371–372, 82–91.

Clark, P.U., Dyke, A.S., Shakun, J.D., Carlson, A.E., Clark, J., Wohlfarth, B., Mitrovica, J.X., Hostetler, S.W., McCabe, A.M., 2009. The last glacial maximum. Science 325, 710–714.

Clement, A.C., Peterson, L.C., 2008. Mechanisms of abrupt climate change of the last glacial period. Rev. Geophys. 46.

Combourieu Nebout, N., Turon, J.L., Zahn, R., Capotondi, L., Londeix, L., Pahnke, K., 2002. Enhanced aridity and atmospheric high-pressure stability over the western Mediterranean during the North Atlantic cold events of the past 50 k.y. Geology 30, 863–866.

Cortijo, E., Labeyrie, L., Vidal, L., Vautravers, M., Chapman, M., Duplessy, J.-C., Elliot, M., Arnold, M., Turon, J.-L., Auffret, G., 1997. Changes in sea surface hydrology associated with Heinrich event 4 in the North Atlantic Ocean between 40° and 60°N. Earth Planet. Sci. Lett. 146, 29–45. https://doi.org/10.1016/S0012-821X(96)00217-8.

de Vernal, A., Rosell-Melé, A., Kucera, M., Hillaire-Marcel, C., Eynaud, F., Weinelt, M., Dokken, T., Kageyama, M., 2006. Comparing proxies for the reconstruction of LGM sea-surface conditions in the northern North Atlantic. Quat. Sci. Rev. 25, 2820–2834. https://doi.org/10.1016/j.quascirev.2006.06.006.

Demény, A., Kern, Z., Czuppon, G., Németh, A., Leél-Őssy, S., Siklósy, Z., Lin, K., Hu, H.-M., Shen, C.-C., Vennemann, T.W., Haszpra, L., 2017. Stable isotope compositions of speleothems from the last interglacial – spatial patterns of climate fluctuations in Europe. Quat. Sci. Rev. 161, 68–80. https://doi.org/10.1016/j.quascirev.2017.02.012.

Denniston, R.F., Houts, A.N., Asmerom, Y., Wanamaker Jr., A.D., Haws, J.A., Polyak, V.J., Thatcher, D.L., Altan-Ochir, S., Borowske, A.C., Breitenbach, S.F.M., Ummenhofer, C.C., Regala, F.T., Benedetti, M.M., Bicho, N.F., 2018. A stalagmite test of North Atlantic SST and Iberian hydroclimate linkages over the last two glacial cycles. Clim. Past 14, 1893–1913. https://doi.org/10.5194/cp-14-1893-2018.

Dickson, R.R., Meincke, J., Malmberg, S.-A., Lee, A.J., 1988. The "great salinity anomaly" in the Northern North Atlantic 1968–1982. Prog. Oceanogr. 20, 103–151. https://doi.org/10.1016/0079-6611(88)90049-3.

Domínguez-Villar, D., Krklec, K., Pelicon, P., Fairchild, I.J., Cheng, H., Edwards, L.R., 2017. Geochemistry of speleothems affected by aragonite to calcite recrystallization – potential inheritance from the precursor mineral. Geochem. Cosmochim. Acta 200, 310–329. https://doi.org/10.1016/j.gca.2016.11.040.

Drysdale, R.N., Zanchetta, G., Hellstrom, J.C., Fallick, A.E., McDonald, J., Cartwright, I., 2007. Stalagmite evidence for the precise timing of North Atlantic cold events during the early last glacial. Geology 35, 77–80.

Dumitru, O.A., Onac, B.P., Polyak, V.J., Wynn, J.G., Asmerom, Y., Fornós, J.J., 2018. Climate variability in the western Mediterranean between 121 and 67 ka derived from a Mallorcan speleothem record. Palaeogeogr. Palaeoclimatol. Palaeoecol. 506, 128–138. https://doi.org/10.1016/j.palaeo.2018.06.028.

Elliot, M., Labeyrie, L., Duplessy, J.C., 2002. Changes in North Atlantic deep-water formation associated with the Dansgaard-Oeschger temperature oscillations (10-60 ka). Quat. Sci. Rev. 21, 1153–1165.

Eynaud, F., de Abreu, L., Voelker, A., Schönfeld, J., Salgueiro, E., Turon, J.-L., Penaud, A., Toucanne, S., Naughton, F., Sánchez Goñi, M.F., Malaizé, B., Cacho, I., 2009. Position of the Polar Front along the western Iberian margin during key cold episodes of the last 45 ka: tracking the PF along the Western Iberian Margin. Geochem. Geophys. Geosyst. 10. https://doi.org/10.1029/2009GC002398.

Fairchild, I.J., Baker, A., 2012. Speleothem Science: from Process to Past Environments. John Wiley & Sons.

Fairchild, I.J., Treble, P.C., 2009. Trace elements in speleothems as recorders of environmental change. Quat. Sci. Rev. 28, 449–468. https://doi.org/10.1016/j.quascirev.2008.11.007.

Fankhauser, A., McDermott, F., Fleitmann, D., 2016. Episodic speleothem deposition tracks the terrestrial impact of millennial-scale last glacial climate variability in SW Ireland. Quat. Sci. Rev. 152, 104–117. https://doi.org/10.1016/j.quascirev.2016.09.019.

Fleitmann, D., Cheng, H., Badertscher, S., Edwards, L.R., Mudelsee, M., Göktürk, O.M., Fankhauser, A., Pickering, R., Raible, C.C., Matter, A., Kramers, J., Tüysüz, O., 2009. Timing and climatic impact of Greenland interstadials recorded in stalagmites from northern Turkey. Geophys. Res. Lett. 36, 1–5.

Fletcher, W.J., Sánchez Goñi, M.F., 2008. Orbital- and sub-orbital-scale climate impacts on vegetation of the western Mediterranean basin over the last 48,000 yr. Quat. Res. 70, 451–464.

Fletcher, W.J., Sánchez Goñi, M.F., Allen, J.R.M., Cheddadi, R., Combourieu-Nebout, N., Huntley, B., Lawson, I., Londeix, L., Magri, D., Margari, V., Müller, U.C., Naughton, F., Novenko, E., Roucoux, K., Tzedakis, P.C., 2010. Millennial-scale variability during the last glacial in vegetation records from Europe. Quat. Sci. Rev. 29, 2839–2864. https://doi.org/10.1016/j.quascirev.2009.11.015.

Frigola, J., Moreno, A., Cacho, I., Canals, M., Sierro, F.J., Flores, J.A., Grimalt, J.O., 2008. Evidence of abrupt changes in Western Mediterranean Deep Water circulation during the last 50kyr: a high-resolution marine record from the Balearic Sea. Quat. Int. 181, 88–104. https://doi.org/10.1016/j.quaint.2007.06.016.

Frisia, S., 2015. Microstratigraphic logging of calcite fabrics in speleothems as tool for palaeoclimate studies. Int. J. Speleol. 44, 1–16.

Frisia, S., Borsato, A., 2010. Karst. In: Alonso-Zarza, A.M., Tanner, L.H. (Eds.), Carbonates in Continental Settings. Facies, Environments and Processes. Developments in Sedimentology 61. Elsevier, Amsterdam, pp. 269–318.

Frisia, S., Borsato, A., Fairchild, I.J., McDermott, F., 2000. Calcite fabrics, growth mechanisms, and environments of formation in speleothems from the Italian Alps and Southwestern Ireland. J. Sediment. Res. 70, 1183–1196.

Frisia, S., Borsato, A., Hellstrom, J., 2018. High spatial resolution investigation of nucleation, growth and early diagenesis in speleothems as exemplar for sedimentary carbonates. Earth Sci. Rev. 178, 68–91. https://doi.org/10.1016/j.earscirev.2018.01.014.

Genty, D., Blamart, D., Ouahdi, R., Gilmour, M.A., Baker, A., Jouzel, J., Van-Exter, S., 2003. Precise dating of Dansgaard-Oeschger climate oscillation in western Europe from stalagmite data. Nature 421, 833–837.

Genty, D., Combourieu-Nebout, N., Peyron, O., Blamart, D., Wainer, K., Mansuri, F., Ghaleb, B., Isabello, L., Dormoy, I., von Grafenstein, U., Bonelli, S., Landais, A., Brauer, A., 2010. Isotopic characterization of rapid climatic events during OIS3 and OIS4 in Villars Cave stalagmites (SW-France) and correlation with Atlantic and Mediterranean pollen records. Quat. Sci. Rev. 29, 2799–2820. https://doi.org/10.1016/j.quascirev.2010.06.035.

Grant, K.M., Rohling, E.J., Ramsey, C.B., Cheng, H., Edwards, R.L., Florindo, F., Heslop, D., Marra, F., Roberts, A.P., Tamisiea, M.E., Williams, F., 2014. Sea-level variability over five glacial cycles. Nat. Commun. 5, 5076. https://doi.org/10.1038/ncomms6076.

Hellstrom, J., McCulloch, M., 2000. Multi-proxy constraints on the climatic significance of trace element records from a New Zealand speleothem. Earth Planet. Sci. Lett. 179, 287–297. https://doi.org/10.1016/S0012-821X(00)00115-1.

Hemming, S.R., 2004. Heinrich events: massive Late Pleistocene detritus layers of the North Atlantic and their global imprint. Rev. Geophys. 42.

Hodell, D.A., Channell, J.E.T., Curtis, J.H., Romero, O.E., Röhl, U., 2008. Onset of "Hudson strait" Heinrich events in the eastern North Atlantic at the end of the middle Pleistocene transition (~640 ka)?: Pleistocene Heinrich events. Paleoceanography 23. https://doi.org/10.1029/2008PA001591.

Hodge, E.J., Richards, D.A., Smart, P.L., Andreo, B., Hoffmann, D.L., Mattey, D.P., González-Ramón, A., 2008. Effective precipitation in southern Spain (266 to 46 kyr) based on a speleothem stable carbon isotope record. Quat. Res. 69, 447–457.

Lachniet, M.S., Denniston, R.F., Asmerom, Y., Polyak, V.J., 2014. Orbital control of western North America atmospheric circulation and climate over two glacial cycles. Nat. Commun. 5.

Laskar, J., Robutel, P., Joutel, F., Gastineau, M., Correia, A.C.M., Levrard, B., 2004. A long-term numerical solution for the insolation quantities of the Earth.

Astron. Astrophys. 428, 261–285.
Lechleitner, F.A., Amirnezhad-Mozhdehi, S., Columbu, A., Comas-Bru, L., Labuhn, I., Pérez-Mejías, C., Rehfeld, K., 2018. The potential of speleothems from western Europe as recorders of regional climate: a critical assessment of the SISAL database. Quaternary 1, 30. https://doi.org/10.3390/quat1030030.
Li, C., Born, A., 2019. Coupled atmosphere-ice-ocean dynamics in Dansgaard-Oeschger events. Quat. Sci. Rev. 203, 1–20. https://doi.org/10.1016/j.quascirev.2018.10.031.
Lynch-Stieglitz, J., 2017. The Atlantic meridional overturning circulation and abrupt climate change. Annu. Rev. Mar. Sci. 9, 83–104. https://doi.org/10.1146/annurev-marine-010816-060415.
Lynch-Stieglitz, J., Schmidt, M.W., Gene Henry, L., Curry, W.B., Skinner, L.C., Mulitza, S., Zhang, R., Chang, P., 2014. Muted change in Atlantic overturning circulation over some glacial-aged Heinrich events. Nat. Geosci. 7, 144–150. https://doi.org/10.1038/ngeo2045.
Mannella, G., Giaccio, B., Zanchetta, G., Regattieri, E., Niespolo, E.M., Pereira, A., Renne, P.R., Nomade, S., Leicher, N., Perchiazzi, N., Wagner, B., 2019. Palaeoenvironmental and palaeohydrological variability of mountain areas in the central Mediterranean region: a 190 ka-long chronicle from the independently dated Fucino palaeolake record (central Italy). Quat. Sci. Rev. 210, 190–210. https://doi.org/10.1016/j.quascirev.2019.02.032.
Margari, V., Gibbard, P.L., Bryant, C.L., Tzedakis, P.C., 2009. Character of vegetational and environmental changes in southern Europe during the last glacial period; evidence from Lesvos Island, Greece. Quat. Sci. Rev. 28, 1317–1339. https://doi.org/10.1016/j.quascirev.2009.01.008.
Margari, V., Skinner, L.C., Tzedakis, P.C., Ganopolski, A., Vautravers, M., Shackleton, N.J., 2010. The nature of millennial-scale climate variability during the past two glacial periods. Nat. Geosci. 3, 127–131. https://doi.org/10.1038/ngeo740.
Martín-García, R., Alonso-Zarza, A.M., Martín-Pérez, A., 2009. Loss of primary texture and geochemical signatures in speleothems due to diagenesis: evidences from Castañar Cave, Spain. Sediment. Geol. 221, 141–149.
Martin-Puertas, C., Brauer, A., Wulf, S., Ott, F., Lauterbach, S., Dulski, P., 2014. Annual proxy data from Lago Grande di Monticchio (southern Italy) between 76 and 112 ka: new chronological constraints and insights on abrupt climatic oscillations. Clim. Past 10, 2099–2114. https://doi.org/10.5194/cp-10-2099-2014.
Martrat, B., Grimalt, J.O., Shackleton, N., de Abreu, L., Hutterli, M.A., Stocker, T.F., 2007. Four climate cycles of recurring deep and surface water destabilizations on the Iberian Margin. Science 317, 502–507.
Martrat, B., Jimenez-Amat, P., Zahn, R., Grimalt, J.O., 2014. Similarities and dissimilarities between the last two deglaciations and interglaciations in the North Atlantic region. Quat. Sci. Rev. 99, 122–134. https://doi.org/10.1016/j.quascirev.2014.06.016.
McCrea, J.M., 1950. On the isotopic chemistry of carbonates and a paleotemperature scale. J. Chem. Phys. 18, 849–857. https://doi.org/10.1063/1.1747785.
McManus, J., Francois, R., Gherardi, J.M., Keigwin, L., Brown-Leger, S., 2004. Collapse and rapid resumption of Atlantic meridional circulation linked to deglacial climate changes. Nature 428, 834–837.
Meyer, M.C., Spötl, C., Mangini, A., 2008. The demise of the Last Interglacial recorded in isotopically dated speleothems from the Alps. Quat. Sci. Rev. 27, 476–496.
Moreno, A., Cacho, I., Canals, M., Prins, M.A., Sánchez-Goñi, M.F., Grimalt, J.O., Weltje, G.J., 2002. Saharan dust transport and high latitude glacial climatic variability: the Alboran Sea record. Quat. Res. 58, 318–328.
Moreno, A., González-Sampériz, P., Morellón, M., Valero-Garcés, B.L., Fletcher, W.J., 2012. Northern Iberian abrupt climate change dynamics during the last glacial cycle: a view from lacustrine sediments. Quat. Sci. Rev. 36, 139–153. https://doi.org/10.1016/j.quascirev.2010.06.031.
Moreno, A., Pérez-Mejías, C., Bartolomé, M., Sancho, C., Cacho, I., Stoll, H., Delgado-Huertas, A., Hellstrom, J., Edwards, R.L., Cheng, H., 2017. New speleothem data from Molinos and Ejulve caves reveal Holocene hydrological variability in northeast Iberia. Quat. Res. 88, 223–233.
Moreno, A., Sancho, C., Bartolomé, M., Oliva-Urcia, B., Delgado-Huertas, A., Estrela, M.J., Corell, D., López-Moreno, J.I., Cacho, I., 2014. Climate controls on rainfall isotopes and their effects on cave drip water and speleothem growth: the case of Molinos cave (Teruel, NE Spain). Clim. Dyn. 43, 221–241. https://doi.org/10.1007/s00382-014-2140-6.
Moreno, A., Stoll, H., Jiménez-Sánchez, M., Cacho, I., Valero-Garcés, B., Ito, E., Edwards, R.L., 2010. A speleothem record of glacial (25–11.6kyr BP) rapid climatic changes from northern Iberian Peninsula. Glob. Planet. Chang. 71, 218–231. https://doi.org/10.1016/j.gloplacha.2009.10.002.
Mori, T., Kashiwagi, K., Amekawa, S., Kato, H., Okumura, T., Takashima, C., Wu, C.-C., Shen, C.-C., Quade, J., Kano, A., 2018. Temperature and seawater isotopic controls on two stalagmite records since 83 ka from maritime Japan. Quat. Sci. Rev. 192, 47–58. https://doi.org/10.1016/j.quascirev.2018.05.024.
Moseley, G.E., Spotl, C., Svensson, A., Cheng, H., Brandstatter, S., Edwards, R.L., 2014. Multi-speleothem record reveals tightly coupled climate between central Europe and Greenland during Marine Isotope Stage 3. Geology 42, 1043–1046. https://doi.org/10.1130/G36063.1.
Müller, U.C., Sánchez Goñi, M.F., 2007. 19. Vegetation dynamics in southern Germany during marine isotope stage 5 (~ 130 to 70 kyr ago). In: Developments in Quaternary Sciences. Elsevier, pp. 277–287. https://doi.org/10.1016/S1571-0866(07)80044-3.
Naughton, F., Sánchez Goñi, M.F., Kageyama, M., Bard, E., Duprat, J., Cortijo, E., Desprat, S., Malaizé, B., Joly, C., Rostek, F., Turon, J.L., 2009. Wet to dry climatic trend in north-western Iberia within Heinrich events. Earth Planet. Sci. Lett. 284, 329–342.
Nehme, C., Verheyden, S., Noble, S.R., Farrant, A.R., Sahy, D., Hellstrom, J., Delannoy, J.J., Claeys, P., 2015. Reconstruction of MIS 5 climate in the central Levant using a stalagmite from Kanaan Cave, Lebanon. Clim. Past 11, 1785–1799. https://doi.org/10.5194/cp-11-1785-2015.
North Greenland Ice Core Project members, 2004. High-resolution record of Northern Hemisphere climate extending into the last interglacial period. Nature 431, 147–151.
Oppo, D.W., McManus, J.F., Cullen, J.L., 2006. Evolution and demise of the last interglacial warmth in the subpolar North Atlantic. Quat. Sci. Rev. 25, 3268–3277. https://doi.org/10.1016/j.quascirev.2006.07.006.
Ortega, R., Maire, R., Devès, G., Quinif, Y., 2005. High-resolution mapping of uranium and other trace elements in recrystallized aragonite–calcite speleothems from caves in the Pyrenees (France): implication for U-series dating. Earth Planet. Sci. Lett. 237, 911–923. https://doi.org/10.1016/j.epsl.2005.06.045.
Pailler, D., Bard, E., 2002. High frequency palaeoceanographic changes during the past 140,000 years recorded by the organic matter in sediments of the Iberian margin. Palaeogeogr. Palaeoclimatol. Palaeoecol. 181, 431–452.
Pérez-Mejías, C., Moreno, A., Sancho, C., Bartolomé, M., Stoll, H., Cacho, I., Cheng, H., Edwards, R.L., 2017. Abrupt climate changes during termination III in southern Europe. Proc. Natl. Acad. Sci. 114, 10047–10052.
Pérez-Mejías, C., Moreno, A., Sancho, C., Bartolomé, M., Stoll, H., Osácar, M.C., Cacho, I., Delgado-Huertas, A., 2018. Transference of isotopic signal from rainfall to dripwaters and farmed calcite in Mediterranean semi-arid karst. Geochem. Cosmochim. Acta 243, 66–98.
Pérez-Mejías, C., Sancho, C., Gázquez, F., Moreno, A., Bartolomé, M., Osácar, M.C., Cheng, H., 2019. Insights into the speleogenesis of Ejulve cave (Iberian Range, NE Spain): quaternary hydrothermal karstification? J. Iber. Geol. 45 (3), 511–527. https://doi.org/10.1007/s41513-019-00107-x.
Pickering, R., Kramers, J.D., Partridge, T., Kodolanyi, J., Pettke, T., 2010. U–Pb dating of calcite–aragonite layers in speleothems from hominin sites in South Africa by MC-ICP-MS. Quat. Geochronol. 5, 544–558. https://doi.org/10.1016/j.quageo.2009.12.004.
Polyak, V.J., Asmerom, Y., Burns, S.J., Lachniet, M.S., 2012. Climatic backdrop to the terminal Pleistocene extinction of North American mammals. Geology 40, 1023–1026. https://doi.org/10.1130/G33226.1.
Rahmstorf, S., 2002. Ocean circulation and climate during the past 120,000 years. Nature 419, 207–214.
Ramsey, C.B., 2008. Deposition models for chronological records. Quat. Sci. Rev. 27, 42–60. https://doi.org/10.1016/j.quascirev.2007.01.019.
Rashid, H., Hesse, R., Piper, D.J.W., 2003. Evidence for an additional Heinrich event between H5 and H6 in the Labrador sea: Heinrich event 5A in the labrador sea. Paleoceanography 18. https://doi.org/10.1029/2003PA000913.
Rasmussen, S.O., Bigler, M., Blockley, S.P., Blunier, T., Buchardt, S.L., Clausen, H.B., Cvijanovic, I., Dahl-Jensen, D., Johnsen, S.J., Fischer, H., Gkinis, V., Guillevic, M., Hoek, W.Z., Lowe, J.J., Pedro, J.B., Popp, T., Seierstad, I.K., Steffensen, J.P., Svensson, A.M., Vallelonga, P., Vinther, B.M., Walker, M.J.C., Wheatley, J.J., Winstrup, M., 2014. A stratigraphic framework for abrupt climatic changes during the Last Glacial period based on three synchronized Greenland ice-core records: refining and extending the INTIMATE event stratigraphy. Dating Synth. Interpret. Palaeoclim. Rec. Model-Data Integr. Adv. Intim. Proj. Ice Core Mar. Terr. Rec. COST Action 106, 14–28. ES0907. https://doi.org/10.1016/j.quascirev.2014.09.007.
Regattieri, E., Giaccio, B., Zanchetta, G., Drysdale, R.N., Galli, P., Nomade, S., Peronace, E., Wulf, S., 2015. Hydrological variability over the Apennines during the Early Last Glacial precession minimum, as revealed by a stable isotope record from Sulmona basin, Central Italy: hydrological variability over the apennines. J. Quat. Sci. 30, 19–31. https://doi.org/10.1002/jqs.2755.
Roberts, N., Jones, M.D., Benkaddour, A., Eastwood, W.J., Filippi, M.L., Frogley, M.R., Lamb, H.F., Leng, M.J., Reed, J.M., Stein, M., Stevens, L., Valero-Garcés, B., Zanchetta, G., 2008. Stable isotope records of Late Quaternary climate and hydrology from Mediterranean lakes: the ISOMED synthesis. Quat. Sci. Rev. 27, 2426–2441.
Roche, D., Paillard, D., Cortijo, E., 2004. Constraints on the duration and freshwater release of Heinrich event 4 through isotope modelling. Nature 432, 379–382.
Rodríguez-Rodríguez, L., Jiménez-Sánchez, M., Domínguez-Cuesta, M.J., Rinterknecht, V., Pallàs, R., Bourlès, D., 2016. Chronology of glaciations in the Cantabrian mountains (NW Iberia) during the last glacial cycle based on in situ-produced 10Be. Quat. Sci. Rev. 138, 31–48. https://doi.org/10.1016/j.quascirev.2016.02.027.
Rossi, C., Mertz-Kraus, R., Osete, M.-L., 2014. Paleoclimate variability during the Blake geomagnetic excursion (MIS 5d) deduced from a speleothem record. Quat. Sci. Rev. 102, 166–180. https://doi.org/10.1016/j.quascirev.2014.08.007.
Rousseau, D.-D., Kukla, G., McManus, J., 2006. What is what in the ice and the ocean? Quat. Sci. Rev. 25, 2025–2030. https://doi.org/10.1016/j.quascirev.2006.03.009.
Rowe, P.J., Mason, J.E., Andrews, J.E., Marca, A.D., Thomas, L., van Calsteren, P., Jex, C.N., Vonhof, H.B., Al-Omari, S., 2012. Speleothem isotopic evidence of winter rainfall variability in northeast Turkey between 77 and 6 ka. Quat. Sci. Rev. 45, 60–72. https://doi.org/10.1016/j.quascirev.2012.04.013.
Ruddiman, W.F., 1977. Late Quaternary deposition of ice-rafted sand in the subpolar North Atlantic (lat 40° to 65°N). Geol. Soc. Am. Bull. 88, 1813. https://doi.org/10.1130/0016-7606(1977)88<1813:LQDOIS>2.0.CO;2.
Sánchez Goñi, M.F., Desprat, S., Daniau, A.-L., Bassinot, F.C., Polanco-Martínez, J.M., Harrison, S.P., Allen, J.R.M., Anderson, R.S., Behling, H., Bonnefille, R., Burjachs, F.,

Carrión, J.S., Cheddadi, R., Clark, J.S., Combourieu-Nebout, N., Mustaphi, C.J.C., Debusk, G.H., Dupont, L.M., Finch, J.M., Fletcher, W.J., Giardini, M., González, C., Gosling, W.D., Grigg, L.D., Grimm, E.C., Hayashi, R., Helmens, K., Heusser, L.E., Hill, T., Hope, G., Huntley, B., Igarashi, Y., Irino, T., Jacobs, B., Jiménez-Moreno, G., Kawai, S., Kershaw, A.P., Kumon, F., Lawson, I.T., Ledru, M.-P., Lézine, A.-M., Liew, P.M., Magri, D., Marchant, R., Margari, V., Mayle, F.E., McKenzie, G.M., Moss, P., Müller, S., Müller, U.C., Naughton, F., Newnham, R.M., Oba, T., Pérez-Obiol, R., Pini, R., Ravazzi, C., Roucoux, K.H., Rucina, S.M., Scott, L., Takahara, H., Tzedakis, P.C., Urrego, D.H., Geel, B.van, Valencia, B.G., Vandergoes, M.J., Vincens, A., Whitlock, C.L., Willard, D.A., Yamamoto, M., 2017. The ACER pollen and charcoal database: a global resource to document vegetation and fire response to abrupt climate changes during the last glacial period. Earth Syst. Sci. Data 9, 679–695.

Sánchez Goñi, M.F., Loutre, M.F., Crucifix, M., Peyron, O., Santos, L., Duprat, J., Malaizé, B., Turon, J.-L., Peypouquet, J.-P., 2005. Increasing vegetation and climate gradient in Western Europe over the Last Glacial Inception (122–110 ka): data-model comparison. Earth Planet. Sci. Lett. 231, 111–130. https://doi.org/10.1016/j.epsl.2004.12.010.

Sánchez-Goñi, M.F., Landais, A., Fletcher, W.J., Naughton, F., Desprat, S., Duprat, J., 2008. Contrasting impacts of Dansgaard-Oeschger events over a western European latitudinal transect modulated by orbital parameters. Quat. Sci. Rev. 27, 1136–1151.

Sánchez-Goñi, M.S., Cacho, I., Turon, J., Guiot, J., Sierro, F., Peypouquet, J., Grimalt, J., Shackleton, N., 2002. Synchroneity between marine and terrestrial responses to millennial scale climatic variability during the last glacial period in the Mediterranean region. Clim. Dyn. 19, 95–105. https://doi.org/10.1007/s00382-001-0212-x.

Sancho, C., Arenas, C., Pardo, G., Peña-Monné, J.L., Rhodes, E.J., Bartolomé, M., García-Ruiz, J.M., Martí-Bono, C., 2018. Glaciolacustrine deposits formed in an ice-dammed tributary valley in the south-central Pyrenees: new evidence for late Pleistocene climate. Sediment. Geol. 366, 47–66. https://doi.org/10.1016/j.sedgeo.2018.01.008.

Sancho, C., Arenas, C., Vázquez-Urbez, M., Pardo, G., Lozano, M.V., Peña-Monné, J.L., Hellstrom, J., Ortiz, J.E., Osácar, M.C., Auqué, L., Torres, T., 2015. Climatic implications of the Quaternary fluvial tufa record in the NE Iberian Peninsula over the last 500ka. Quat. Res. 84, 398–414.

Scholz, D., Tolzmann, J., Hoffmann, D.L., Jochum, K.P., Spötl, C., Riechelmann, D.F.C., 2014. Diagenesis of speleothems and its effect on the accuracy of 230Th/U-ages. Chem. Geol. 387, 74–86. https://doi.org/10.1016/j.chemgeo.2014.08.005.

Sierro, F.J., Hodell, D.A., Curtis, J.H., Flores, J.A., Reguera, I., Colmenero-Hidalgo, E., Bárcena, M.A., Grimalt, J.O., Cacho, I., Frigola, J., Canals, M., 2005. Impact of iceberg melting on Mediterranean thermohaline circulation during Heinrich events. Paleoceanography 20. https://doi.org/10.1029/2004PA001051.

Sirocko, F., Seelos, K., Schaber, K., Rein, B., Dreher, F., Diehl, M., Lehne, R., Jäger, K., Krbetschek, M., Degering, D., 2005. A late Eemian aridity pulse in central Europe during the last glacial inception. Nature 436, 833–836.

Spötl, C., 2011. Long-term performance of the Gasbench isotope ratio mass spectrometry system for the stable isotope analysis of carbonate microsamples. Rapid Commun. Mass Spectrom. 25, 1683–1685. https://doi.org/10.1002/rcm.5037.

Springer, G.S., Rowe, H.D., Hardt, B., Cheng, H., Edwards, R.L., 2014. East central North America climates during marine isotope stages 3-5: East-Central North America climates. Geophys. Res. Lett. 41, 3233–3237. https://doi.org/10.1002/2014GL059884.

Stoll, H., Mendez-Vicente, A., Gonzalez-Lemos, S., Moreno, A., Cacho, I., Cheng, H., Edwards, R.L., 2015. Interpretation of orbital scale variability in mid-latitude speleroothem δ18O: significance of growth rate controlled kinetic fractionation effects. Quat. Sci. Rev. 127, 215–228. https://doi.org/10.1016/j.quascirev.2015.08.025.

Stoll, H.M., Moreno, A., Mendez-Vicente, A., Gonzalez-Lemos, S., Jimenez-Sanchez, M., Dominguez-Cuesta, M.J., Edwards, R.L., Cheng, H., Wang, X., 2013. Paleoclimate and growth rates of speleothems in the northwestern Iberian Peninsula over the last two glacial cycles. Quat. Res. 80, 284–290.

Toucanne, S., Angue Minto'o, C.M., Fontanier, C., Bassetti, M.-A., Jorry, S.J., Jouet, G., 2015. Tracking rainfall in the northern Mediterranean borderlands during sapropel deposition. Quat. Sci. Rev. 129, 178–195. https://doi.org/10.1016/j.quascirev.2015.10.016.

Tzedakis, C., 2005. Towards an understanding of the response of southern European vegetation to orbital and suborbital climate variability. Quat. Sci. Rev. 24, 1585–1599.

Tzedakis, P.C., Drysdale, R.N., Margari, V., Skinner, L.C., Menviel, L., Rhodes, R.H., Taschetto, A.S., Hodell, D.A., Crowhurst, S.J., Hellstrom, J.C., Fallick, A.E., Grimalt, J.O., McManus, J.F., Martrat, B., Mokeddem, Z., Parrenin, F., Regattieri, E., Roe, K., Zanchetta, G., 2018. Enhanced climate instability in the north Atlantic and southern Europe during the last interglacial. Nat. Commun. 9, 4235. https://doi.org/10.1038/s41467-018-06683-3.

Vansteenberge, S., Verheyden, S., Cheng, H., Edwards, R.L., Keppens, E., Claeys, P., 2016. Paleoclimate in continental northwestern Europe during the Eemian and early Weichselian (125–97 ka): insights from a Belgian speleothem. Clim. Past 12, 1445–1458. https://doi.org/10.5194/cp-12-1445-2016.

Vautravers, M.J., Shackleton, N.J., 2006. Centennial-scale surface hydrology off Portugal during marine isotope stage 3: insights from planktonic foraminiferal fauna variability: off Portugal during MIS 3. Paleoceanography 21. https://doi.org/10.1029/2005PA001144.

Vautravers, M.J., Shackleton, N.J., Lopez-Martinez, C., Grimalt, J.O., 2004. Gulf Stream variability during marine isotope stage 3: gulf Stream variability. Paleoceanography 19. https://doi.org/10.1029/2003PA000966.

Vegas, J., Ruiz-Zapata, B., Ortiz, J.E., Galán, L., Torres, T., García-Cortés, Á., Gil-García, M.J., Pérez-González, A., Gallardo-Millán, J.L., 2010. Identification of arid phases during the last 50 cal. ka BP from the Fuentillejo maar-lacustrine record (Campo de Calatrava Volcanic Field, Spain). J. Quat. Sci. 25, 1051–1062. https://doi.org/10.1002/jqs.1262.

Veres, D., Lallier-Vergès, E., Wohlfarth, B., Lacourse, T., Kéravis, D., Björck, S., Preusser, F., Andrieu-Ponel, Val., Ampel, L., 2009. Climate-driven changes in lake conditions during late MIS 3 and MIS 2: a high-resolution geochemical record from Les Echets, France. Boreas 38, 230–243. https://doi.org/10.1111/j.1502-3885.2008.00066.x.

Voelker, A.H.L., Abreu, L., 2011. A review of abrupt climate change events in the northeastern 631 Atlantic Ocean (Iberian margin): latitudinal, longitudinal, and vertical gradients. In: Rashid, H., Polyak, L., Mosley-Thompson, E. (Eds.), Abrupt Climate Change: Mechanisms, Patterns, and Impacts. Geophysical Monograph Series.

Vogel, H., Wagner, B., Zanchetta, G., Sulpizio, R., Rosén, P., 2010. A paleoclimate record with tephrochronological age control for the last glacial-interglacial cycle from Lake Ohrid, Albania and Macedonia. J. Paleolimnol. 44, 295–310. https://doi.org/10.1007/s10933-009-9404-x.

Wainer, K., Genty, D., Blamart, D., Bar-Matthews, M., Quinif, Y., Plagnes, V., 2013. Millennial climatic instability during penultimate glacial period recorded in a south-western France speleothem. Palaeogeogr. Palaeoclimatol. Palaeoecol. 376, 122–131. https://doi.org/10.1016/j.palaeo.2013.02.026.

Wainer, K., Genty, D., Blamart, D., Daëron, M., Bar-Matthews, M., Vonhof, H., Dublyansky, Y., Pons-Branchu, E., Thomas, L., van Calsteren, P., Quinif, Y., Caillon, N., 2011. Speleothem record of the last 180 ka in Villars cave (SW France): investigation of a large [delta]18O shift between MIS6 and MIS5. Quat. Sci. Rev. 30, 130–146. https://doi.org/10.1016/j.quascirev.2010.07.004.

Wainer, K., Genty, D., Blamart, D., Hoffmann, D., Couchoud, I., 2009. A new stage 3 millennial climatic variability record from a SW France speleothem. Palaeogeogr. Palaeoclimatol. Palaeoecol. 271, 130–139.

Weber, M., Scholz, D., Schröder-Ritzrau, A., Deininger, M., Spötl, C., Lugli, F., Mertz-Kraus, R., Jochum, K.P., Fohlmeister, J., Stumpf, C.F., Riechelmann, D.F.C., 2018. Evidence of warm and humid interstadials in central Europe during early MIS 3 revealed by a multi-proxy speleothem record. Quat. Sci. Rev. 200, 276–286. https://doi.org/10.1016/j.quascirev.2018.09.045.

Wolf, D., Kolb, T., Alcaraz-Castaño, M., Heinrich, S., Baumgart, P., Calvo, R., Sánchez, J., Ryborz, K., Schäfer, I., Bliedtner, M., Zech, R., Zöller, L., Faust, D., 2018. Climate deteriorations and Neanderthal demise in interior Iberia. Sci. Rep. 8. https://doi.org/10.1038/s41598-018-25343-6.

Wolff, E.W., Chappellaz, J., Blunier, T., Rasmussen, S.O., Svensson, A., 2010. Millennial-scale variability during the last glacial: the ice core record. Quat. Sci. Rev. 29, 2828–2838. https://doi.org/10.1016/j.quascirev.2009.10.013.

Wulf, S., Brauer, A., Kraml, M., Keller, J., Negendank, J.F.W., 2004. Tephrochronology of the 100 ka lacustrine sediment record of Lago Grande di Monticchio (southern Italy). Quat. Int. 122, 7–30.

Wulf, S., Hardiman, M.J., Staff, R.A., Koutsodendris, A., Appelt, O., Blockley, S.P.E., Lowe, J.J., Manning, C.J., Ottolini, L., Schmitt, A.K., Smith, V.C., Tomlinson, E.L., Vakhrameeva, P., Knipping, M., Kotthoff, U., Milner, A.M., Müller, U.C., Christanis, K., Kalaitzidis, S., Tzedakis, P.C., Schmiedl, G., Pross, J., 2018. The marine isotope stage 1–5 cryptotephra record of Tenaghi Philippon, Greece: towards a detailed tephrostratigraphic framework for the Eastern Mediterranean region. Quat. Sci. Rev. 186, 236–262. https://doi.org/10.1016/j.quascirev.2018.03.011.